

Review

Surface Modification of Biochar for Dye Removal from Wastewater

Lalit Goswami , Anamika Kushwaha , Saroj Raj Kafle  and Beom-Soo Kim *

Department of Chemical Engineering, Chungbuk National University, Cheongju 28644, Korea; lalitgoswami660323@gmail.com (L.G.); kushwaha.anamika@gmail.com (A.K.); 100sarojraj@gmail.com (S.R.K.)
* Correspondence: bskim@chungbuk.ac.kr

Abstract: Nowadays, biochar is being studied to a great degree because of its potential for carbon sequestration, soil improvement, climate change mitigation, catalysis, wastewater treatment, energy storage, and waste management. The present review emphasizes on the utilization of biochar and biochar-based nanocomposites to play a key role in decontaminating dyes from wastewater. Numerous trials are underway to synthesize functionalized, surface engineered biochar-based nanocomposites that can sufficiently remove dye-contaminated wastewater. The removal of dyes from wastewater via natural and modified biochar follows numerous mechanisms such as precipitation, surface complexation, ion exchange, cation- π interactions, and electrostatic attraction. Further, biochar production and modification promote good adsorption capacity for dye removal owing to the properties tailored from the production stage and linked with specific adsorption mechanisms such as hydrophobic and electrostatic interactions. Meanwhile, a framework for artificial neural networking and machine learning to model the dye removal efficiency of biochar from wastewater is proposed even though such studies are still in their infancy stage. The present review article recommends that smart technologies for modelling and forecasting the potential of such modification of biochar should be included for their proper applications.

Keywords: post-processing modification; surface-engineered biochar; dye removal; machine learning; artificial neural network



Citation: Goswami, L.; Kushwaha, A.; Kafle, S.R.; Kim, B.-S. Surface Modification of Biochar for Dye Removal from Wastewater. *Catalysts* **2022**, *12*, 817. <https://doi.org/10.3390/catal12080817>

Academic Editor: John Vakros

Received: 2 July 2022

Accepted: 22 July 2022

Published: 26 July 2022

Publisher's Note: MDPI stays neutral with regard to jurisdictional claims in published maps and institutional affiliations.



Copyright: © 2022 by the authors. Licensee MDPI, Basel, Switzerland. This article is an open access article distributed under the terms and conditions of the Creative Commons Attribution (CC BY) license (<https://creativecommons.org/licenses/by/4.0/>).

1. Introduction

Unprecedented rising globalization, industrialization, urbanization, and anthropogenic human activities have led to a worldwide shortage of clean water [1–3]. In this regard, wastewater contaminated by water-soluble dyes is one of the prime environmental issues [4–6]. Nowadays, numerous dyes and additives are being utilized enormously in industrial applications such as textile, paper, printing, paint, laundry, cosmetics, carpet, leather, food, and rubber [4]. Globally, more than 10,000 different types of natural and synthetic dyes are produced annually, weighing in the range of 7×10^5 – 1×10^6 tons [7]. The chemical complexity, stability, and poor biodegradability of these dye-contaminated wastewaters are of prime concern and continue to limit the clean water resources available. The rising demand for dyes is simultaneously leading to the malefactors of inadvertent discharge of dye-contaminated wastewater into water streams; it directly affects the life of aquatic flora and fauna along with the food chain and is indirectly deleterious to human health [8–10]. Henceforth, it is highly significant to develop sustainable remediation solutions to remove soluble dyes and other contaminants from water.

It typically costs about \$1 billion annually to treat 640 million m³ of textile and dyeing wastewater [11]. Several conventional dye-contaminated wastewater treatment technologies are used for dye removal from effluents, such as chemisorption, electrochemical oxidation, ozonation, ion exchange, membrane filtration, anaerobic lagoons, sedimentation, oxidation ponds, coagulation flocculation, photocatalytic degradation, and gamma irradiation [4,11–13]. Among these treatments, adsorption is one of the most sustainable

and cost-effective techniques because other technologies require a lot of chemicals, high energy, and are not cost effective. Carbonaceous materials possessing a high specific surface area (SSA) are widely used as adsorbing agents in wastewater treatment for dye removal [14,15]. Inexpensive adsorbents, preferably derived from natural materials and industrial wastes/by-products, such as biochar, cellulose, aerogels, activated charcoal, bentonite, fly ash, and silica, can be utilized for wastewater treatment [16–20].

Biochar (BC) is a highly stable carbonaceous material that is aromatized and amorphous in nature. It is usually formed after thermochemical conversion of organic matter and wastes at temperatures of 350–750 °C under limited oxygen conditions [21–23]. Its high SSA, pore volume, hydrophobicity, etc., enable its use as an efficient biomaterial for carbon sequestration, soil improvement, climate change mitigation, catalysis, wastewater treatment, energy storage, and waste management [4]. In addition, it has been well recognized as a potentially highly efficient, low-cost, and eco-friendly adsorbent for the removal of organic and inorganic pollutants, particularly heavy metals and dyes from wastewater.

The physicochemical properties and primary composition of BC are considerably altered according to the biomass feedstock, carbonization procedure, degree of pyrolysis, activation, and functionalization techniques [23]. Indulging in modification techniques, BC depicts multiscale porous structures, extensive surface functional groups, and high surface areas, utilizing various organic feedstocks. In addition, inherent functional sites (hydroquinone, defects, etc.) and minerals (silica, transition metals) add BC as a promising ingredient to tailor heterojunctions/composites. The facile metal impregnation, gas activation, sulfonation, and ionic liquid grafting of BC enable many advantages in catalytic processes owing to enhanced accessibility to active sites, excellent π - π interactions, high active surface area, and enhanced charge transfer [24].

In this review, we focused on surface modification and alteration of BC to enhance the efficiency of dye removal from wastewater. A network visualization of terms associated with biochar and dye with a minimum number of 10 occurrences of 3589 associated keywords is represented in Figure 1 (assessed 30 June 2022). It represents the current trends in research related to the application of biochar in association with dye in the Web of Science. Here, the various colors of the nodes represent different clusters, while the size of each bubble depicts its frequency of occurrence. A literature review of BC reports that thermochemical conversion often exhibits low reactivity and selectivity for dye removal [25]. To eliminate these limitations, BC is tailored via numerous techniques to achieve the desired selectivity and reactivity to enhance surface sites and hydrophobicity for regulating the dye removal kinetics [26–28]. Factors affecting BC properties and various post-processing modifications, functionalization, and BC activation for dye removal are included. Literature review reports on surface modification of BC for dye removal are very scarce. The application of smart digital technologies such as machine learning and artificial neural networks (ANN) is also covered to further enhance dye removal via BC.

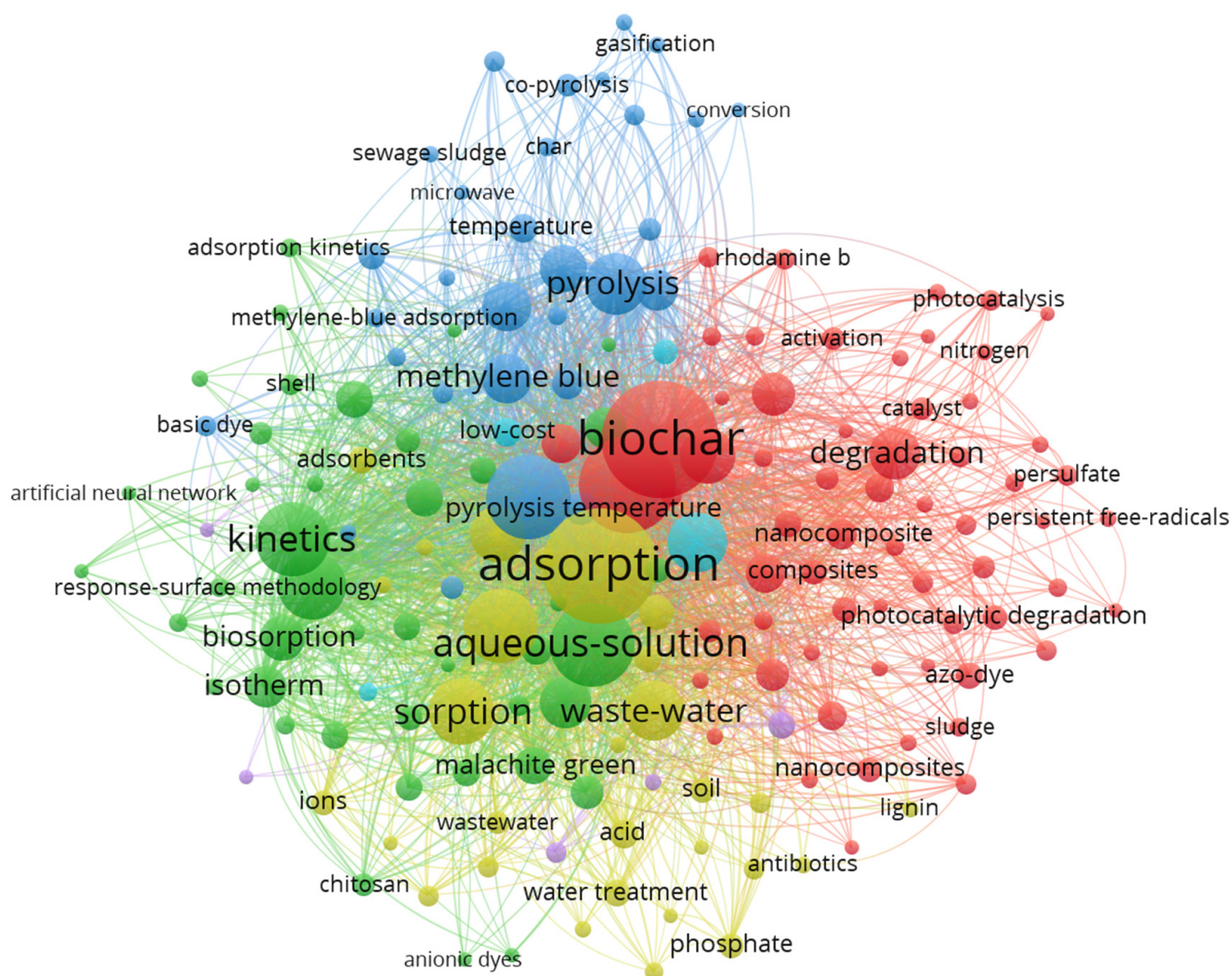


Figure 1. Network visualization of terms associated with biochar and dye.

2. Biochar

2.1. Production of Biochar

Various methods have been employed for BC production, such as combustion, torrefaction, gasification, and pyrolysis (slow and fast types) [29]. Each method results in a different char yield and carbon level. These processes differ based on temperature, char yield, heating rate, feedstock residence time, and carbon content and yield. Earlier, combustion was used to produce charcoal from woody biomass; however, it resulted in low yields and extreme air pollution. With time, the advancement in technology (endothermic and exothermic processes) allows the maximum energy extraction from organic matter. Combustion and gasification generate heat and gas, respectively, by thermally decomposing organic matter in an oxic environment [30]. However, these processes are less effective and satisfactory in decreasing emissions while meeting energy requirements. On the other hand, pyrolysis is the most common, oldest, and the most effective process for meeting energy requirements and reducing emissions. Figure 2 depicts the mechanism of BC formation from cellulose, hemicellulose, and lignin [31]. Pyrolysis leads to the production of BC (solid), bio-oil (liquid), and syngas (gas). The generated by-products can also be utilized as energy substances to meet the energy crisis.

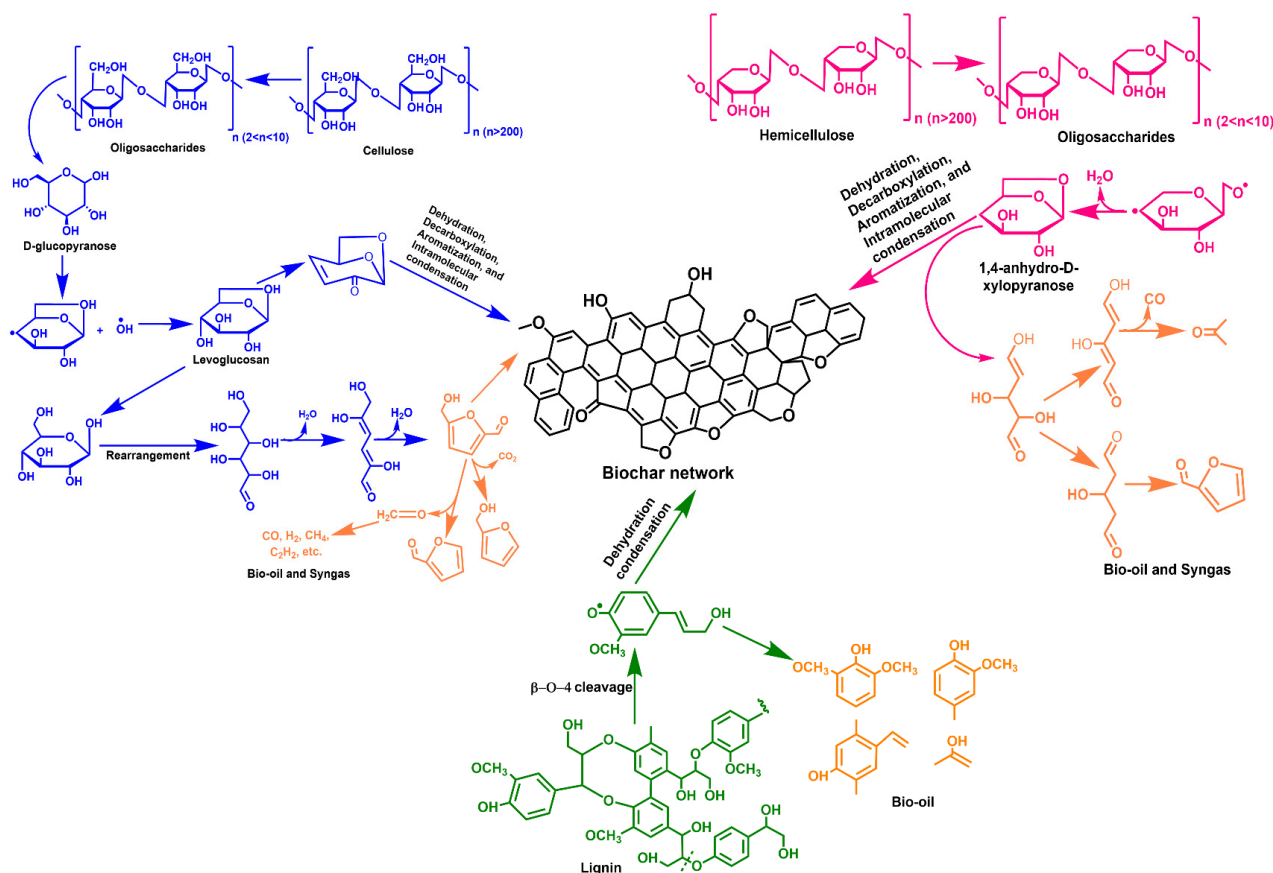


Figure 2. Mechanism of biochar formation from cellulose, hemicellulose, and lignin.

Here, pyrolysis can be classified into slow, intermediate, and fast pyrolysis in accordance with the heating rate, temperature, pressure, and residence time [23]. For high yield of BC, slow pyrolysis should meet heating rate of $0.1\text{--}1\text{ }^{\circ}\text{C min}^{-1}$, whereas fast pyrolysis and high temperature can result in generation of more liquid and syngas. In addition, the mass fraction range of pyrolysis solid increases with increasing temperature. In case of intermediate pyrolysis where the conditions are between slow and fast pyrolysis, there is a balance yield of BC and bio-oil yield, but it is rarely approved from a BC production perspective [32,33]. Further, the properties of BC depend on numerous factors and parameters such as pyrolysis temperature and type of feedstock.

Some conceivable approaches for more efficient BC production are proposed as follows: (i) improving energy efficiency via utilization of batch reactors through continuous feeding pyrolyzers; (ii) enhancing energy efficiency and BC yield using exothermic operation; (iii) tuning the BC properties (texture feature and surface chemistry) by adjusting the operating conditions; (iv) improving process economics and reducing pollutant emissions; (v) exploring new biomass-based feedstocks [34].

2.2. Characteristics of Biochar

2.2.1. Physical Properties

The physical properties of BC are directly dependent on the biomass feedstock and pyrolysis conditions, including biomass pre-treatment and handling. In particular, the attrition, crack formation, and microstructural rearrangement generated under different pyrolysis conditions change the native structure of the biomass feedstock to varying degrees [34]. As the pyrolysis process progresses, the biomass feedstock is reduced, converting macropores into mesopores and micropores. The ideal BC physical structure can be enhanced by increasing the pyrolysis temperatures to the point where deformation occurs [35]. Thermal decomposition of organic materials begins at $>120\text{ }^{\circ}\text{C}$. More specifically,

hemicellulose, cellulose, and lignin decompose at 200–260 °C, 240–350 °C, and 280–500 °C, respectively.

Nano and Macroporosity

The pore size distribution is one of the most important physical properties. Macropores (>50 nm), mesopores (2–50 nm), and micropores (<2 nm) constitute the total pore volume of BC. Here, micropores are the prime contributors to the BC surface area and are also responsible for efficient adsorbents, whereas mesopores play a noteworthy role in the liquid–solid adsorption process [24,34]. Further, micropores are amended via prolonging pyrolysis at higher temperatures which simultaneously release the volatile content of the feedstock along with the creation of numerous pores. Slow pyrolysis enhances the porosity of BC via slow decomposition of lignin content. The surface area of BC increases quickly when the pyrolysis temperature exceeds >400 °C, owing to thermal condensation of the biomass feedstock and micropore formation [35]. Biomass possessing aromatic lignin cores, aliphatic alkyl, and ester groups produces a higher surface area when pyrolyzed at higher temperatures.

Particle Size Distribution

BC particle size is determined by biomass rigidity against shrinkage and slow destruction during the pyrolysis process. Usually, the BC particle sizes are smaller compared to the un-pyrolyzed biomass. However, agglomeration may occur during pyrolysis, resulting in BC with a larger particle size [34]. Post-mechanical stresses may also occur, crumbling BC more susceptible than the original biomass. Slow pyrolysis (5–30 °C/min) results in a smaller size of BC. BC particle size has an inverse correlation with reaction temperature. For instance, an increase in reaction temperature (450 °C to 700 °C) results in the formation of smaller size particles [23]. This could be due to the augmented susceptibility to attrition because of the lower biomass/BC tensile strength [36].

Density

Apparent/bulk/solid density can be evaluated relating to determining the physical properties of BC. Usually, there is an antagonistic relationship between bulk density and solid density. In general, the solid density of BC is higher than that of the original biomass as a result of the release of volatile and condensable compounds and the formation of graphitic crystallites [34,36]. In contrast, BC has a lower bulk density compared to wood precursor owing to biomass drying and carbonization.

Mechanical Strength

This property correlates directly with density and inversely with porosity. Few studies have reported the evaluation of mechanical strength of BC [37]. In comparison to the virgin wood, monolithic carbonized wood BC has lower stiffness (37%) and higher strength (28%). Here, both the reduced modulus and hardness of pyrolyzed wood BC incessantly increases with increasing temperature (between 700 and 2000 °C) [38]. A negative effect on these properties follows with a further increase in the pyrolysis temperature. In addition, compared to harder native woods (low ash and high lignin content), fruit stones/pits and nutshells are more appreciated for BC production depicting admirable mechanical properties [34]. Further, it was found that the pyrolytic temperature is more dominant than the residence time in determining the mechanical properties of BC.

2.2.2. Chemical Properties

BC properties depend on the biomass type and pyrolysis temperature. In fact, data on synthesis techniques can be used to predict the properties and functions of BC [39]. In general, with a surge in pyrolysis temperature, BC yield declines exponentially while BC alkalinity (pH) displays a linear rise [34,39]. The increase in pH can be ascribed to thermal decomposition of hydroxyl groups and other weak bonds within the BC structure at high

temperatures. In comparison, due to the removal of acidic functional groups, the cation exchange capacity of BC is inversely proportional to the pyrolysis temperature [34,39]. BC derived from biosolids display the highest cation exchange capacity due to the presence of minerals (P, Mg, Ca, Na, and K) in the biosolids, which encourage the generation of oxygen-containing functional groups on the surface of BC [40]. Unlike ash, the volatile matter content of BC decreases linearly with increasing pyrolysis temperature. Ash formation is due to inorganic minerals remaining following the decomposition of H, O, and C of biomass [39]. The destruction of hydroxyl, azanide, and other weakly bonded groups results in the reduction of these elements with increasing temperature. However, the C content gradually declines, resulting in a higher C content in the BC at the enhanced pyrolysis temperatures [39].

2.2.3. Microchemical Characteristics

BC microchemical properties can influence its superficial sorption characteristics. The microchemical properties vary significantly depending on the nature and composition of solid phase, entrapped oils and their arrangement, and indicate the electrochemical properties and functional groups on the BC surface [34,41]. Dried biomass pyrolysis is activated by hemolytic cleavage of covalent bonds to release free radicals and structural O [41]. In the initial phases of pyrolysis, free radicals are generated from low atmospheric O₂ levels [34,40,41]. This process proceeds with the formation of carboxyl and carbonyl groups, followed by their cleavage into CO₂ and CO. Finally, BC residues are produced from free radical fragments that recombine with the substrate in various ways [41].

2.2.4. Organo-Chemical Characteristics

In general, the H-to-C ratio declines from ~ 1.5 to ≤ 0.5 in lignocellulosic biomass with pyrolysis temperatures of >400 °C. This reduction in the H-to-C ratio could be due to changes in the elemental (N, O, H, and C) content during thermal decomposition of the biomass. O-to-C and H-to-C ratios (displaying the degree of aromaticity and maturation) in BC decrease at higher reaction temperatures [23,34]. Burnt peat displayed an H-to-C ratio of 1.3 when the maximum C content was either associated through a hydroxyl group or directly bonded to a proton. If the H-to-C ratio drops to 0.4–0.6, it indicates that every second to third C is associated with a proton [34].

2.3. Factors Influencing Biochar Sorption Efficiency

BC is a carbonaceous material derived via biomass thermal conversion (pyrolysis, gasification, hydrothermal carbonization, and torrefaction) under oxygen-limited conditions [4]. Typically, cellulose (40–60%), hemicellulose (20–40%), and lignin (10–25%) are included within biomass [5]. Biomass structural building blocks undergo a sequence of reactions during thermal decomposition, such as dehydration, de-polymerization, rearrangement, re-polymerization, condensation, and carbonization at various temperatures, producing BC, bio-oil, and syngas [22]. Based on the feedstock, the desired product and its application vary. Biomass characteristics include elemental composition, size, and ash mineral content, whereas thermal conditions include temperature, heating rate, pressure, and residence time [11,23]. Several parameters affect BC performance during adsorption. BC physisorption isotherm characteristics govern properties such as morphological structure and reactivity depending on pyrolytic conditions.

2.3.1. Temperature

Reaction temperature plays a vital role in the process and reaction rate. Huang et al. [42] suggested that the adsorption is chemical rather than physical when the equilibrium temperature does not significantly affect the adsorption process. Based on the pore size, adsorbent materials of various sizes are grouped into micropores, mesopores, and macropores, which are highly dependent upon the production conditions of BC. BC produced by pyrolysis at high temperatures contains high micropore volumes ranging

from 50% to 70% of the total pores. Adsorption of contaminants by BC is an endothermic process and the adsorption capacity increases with increasing temperature.

An experimental study was conducted by Tan et al. [43] on Cu (II) adsorption and textile dye adsorption into food waste BC, and thermodynamics parameters were calculated. In both cases, the heat of reaction was positive and Gibbs's free energy was negative. According to Ambaye et al. [44], as the reaction temperature increases, the BC surface area increases as the amount of oxygen-containing functional groups on the surface decreases. Wu et al. [45] used litchi peel biomass and increased the activated temperature from 650 °C to 850 °C, which ultimately increased the surface area from 531 m² g⁻¹ to 1006 m² g⁻¹ and the pore volume from 0.328 cm³ g⁻¹ to 0.588 cm³ g⁻¹.

One experimental setup was carried out by Qambrani et al. [46] to perceive the effect of temperature on BC yield and quality. The yield, total nitrogen and organic carbon content, and cation exchange capacity values were found to decrease with increasing pyrolysis temperature. Therefore, low temperatures are highly recommended for BC production from poultry litter. This condition applies analogously to the condition for BC obtained from vegetative materials.

2.3.2. Solution pH

Solution pH plays a vital role in controlling the surface charge of the adsorbent and the degree of ionization of adsorbate [47]. At high pH, a negative charge exists on the surface with deprotonation of the phenolic and carboxylic groups. At low pH, basic functional groups become protonated and positively charged, promoting adsorption of anions. Adsorption by BC is known to be a function of pH, medium, and deprotonation of functional groups [48]. The pH at the zero-point change is the point at which the net charge on the surface of any adsorbent in solution becomes neutral. At this point, pH highly affects the adsorption efficiency of the BC active surface by providing active functional groups for a charged solution. Therefore, increasing the pH of a solution containing BC leads to a negative potential by increasing the negative charge on the BC surface [49].

Qiu et al. [50] reported that the positive charge on activated carbon at pH 3.0 was higher than at pH 6.5. In contrast, the negative charge on BC was more negative at pH 6.5. Therefore, BC was more efficient than activated carbon at adsorbing dyes from solution. Similarly, the effect of pH on methylene blue dye adsorption was studied at various pH (2–10) [51]. As the pH increases, the number of positively charged sites decreases, increasing methylene blue adsorption. Although the high adsorption of the methylene blue is favorable in alkaline solution, the adsorption did not change when the pH of the solution increased. They observed a maximum dye adsorption (69.07%) at pH 4 [51]. Lin et al. [52] tested the microalgae derivative BC to remove dye and found that the higher the pH of the aqueous solution, the greater the adsorption capacity of positively charged dyes with surface electrostatic attraction due to the negative potential effects. Similarly, Huang et al. [53] studied the removal of organic dye using BC derived from *Spirulina platensis* algae biomass residue. The maximum adsorption capacity was obtained at the alkaline pH with an adsorbent dosage of 2000 mg/L and an initial dye concentration of 90 mg/L.

2.3.3. Adsorbent Dosage

The adsorbent dosage greatly influences the sorbent-sorbate equilibrium in the adsorption system. Due to the availability of more sorption sites, the removal efficiency of organic and inorganic pollutants increases with increasing adsorbent dosage. When the dosage rate is in excess, the adsorption capacity of BC decreases [48]. The reduction in adsorption may be attributed to the overlap of adsorption sites which ultimately shield the pores [48]. Moreover, at a lower dosage of adsorbent at a given initial dye concentration, the ratio of dye to adsorbent molecules increases, leading to an increase in specific uptake. In contrast, at a higher dosage of adsorbent, the availability of dye ions is insufficient for adsorption to the sites [53].

The effect of adsorbent dosage of BC derived from eucalyptus bark to remove methylene blue dye from aqueous solution was studied [53]. They observed that the dye adsorption decreased from 56.8 to 25.5 (mg/g) as the adsorbent dosage was increased from 0.01 to 0.03 g. According to Zhang et al. [54], Congo red dye removal (82.2–83.6%) increased as the adsorbent dosage was increased from 0.2 to 1 g/100 mL. Green BC composite was used for methylene blue removal with adsorbent doses up to 2 g/L. It was found that the adsorption performance decreases with increasing dosage, reducing the number of methylene blue molecules per unit adsorbent [54].

2.3.4. Initial Dye Concentration

For an efficient and effective adsorption process, the initial concentration of adsorbate plays a vital role. As the initial dye concentration increases, the percentage removal of dye increases. The initial dye concentration provides the driving force to overcome the mass transfer resistance of dye between the aqueous and solid phases [51]. According to Chowdhury et al. [55], at high concentrations, all dye molecules in solution do not interact with the binding sites of the adsorbent because the adsorbent has a limited number of active binding sites that saturate at a certain concentration. Experimental work carried out by Dawood et al. [56] found that the percentage of methylene blue removal decreased from 80.5% to 36.8% as the initial concentration (10–100 mg/L) of the methylene blue dye solution increased. Another experimental work was also carried out in which the percentage removal of methylene blue dye drastically reduced from 85.93% to 41.40% with increasing initial dye concentration (20 to 50 mg/L) [57].

2.3.5. Heating Rate

The heating rate is also one of the major factors affecting BC properties. According to Xu and Chen [58], heating rates of $<20\text{ }^{\circ}\text{C s}^{-1}$ for BC production from pine sawdust permitted the natural porosity of sawdust to be shifted to BC without significant structural variations. In contrast, devolatilization occurred at a heating rate of $500\text{ }^{\circ}\text{C s}^{-1}$, resulting in deformation of the sawdust cell structure. Finally, lower pyrolysis temperature and lower heating rate along with high residence time led to BC formation. Li et al. [59] produced BC from lignin (heating rate of $10\text{ }^{\circ}\text{C min}^{-1}$) and the abundance of -OH started to decrease from $350\text{ }^{\circ}\text{C}$. They concluded that a lower heating rate with long residence time increased the thermal stability of the -OH functional groups on the BC surface. BC carbon content increased from 75.39% to 88.35%, 75.15% to 88.28%, and 77.13% to 89.70% at various heating rates 5, 10, and $15\text{ }^{\circ}\text{C min}^{-1}$, respectively. Li et al. [59] concluded that the smaller particle size leads to a complete pyrolysis process, and the hydrogen, sulfur, and oxygen content decreases with increasing temperature. With an upsurge in temperature, the H/C and O/C atoms gradually decrease and BC becomes more carbonaceous and aromatic.

2.3.6. Particle Size

The rate of heat and mass transfer of particles and the degree of subordinate reactions are significantly influenced by the particle size of the biomass. The particle size depends on the process being carried out and the feedstock materials. Larger particle sizes ($>1.8\text{ mm}$) have greater temperature gradients and thus provide higher BC in comparison with smaller particle sizes [46]. An experiment was conducted with various particle sizes of wood, and it was observed that maximum BC yield (28%) was attained with particle sizes 0.224–0.425 mm at $500\text{ }^{\circ}\text{C}$ and $223.15\text{ }^{\circ}\text{C min}^{-1}$ heating rate in an inert environment [60]. Mechanical properties such as mechanical strength, yield stress, and BC density are highly dependent on biomass particle size. As a result of examining the effect of particle size on wood biomass, it was found that wood BC produced from smaller particle sizes showed higher yield stress and density compared to larger ones [61]. The smaller particle size is appropriate for fast pyrolysis due to the uniform and effective heat transfer facilitating the release of volatiles.

2.3.7. Feedstock Composition

Feedstock selections also greatly impact BC properties and elemental composition. It affects various physical properties of BC, such as pH, pore structure, surface area, adsorption efficiency, and other chemical properties [34]. Compared to cellulose, hemicellulose, lignin, and some organic compounds, a feedstock consisting of animal manure results in higher BC nutrients. As the temperature increases, the volatile compounds in the biomass decrease along with a decrease in the quantity of surface functional groups, but the surface area and ash content of BC increase [23,24]. Feedstock materials are oxygen-rich and hydrogen-deprived, for example, sugars are non-graphitizing and create robust cross-linked arrangements that immobilize the structure and tie the crystallites into a stiff mass. The various carbon and nitrogen contents in char produced from plant-derived biomass were found to be increased relative to biomass. However, the use of mineral-rich feedstock (manure) may reduce it [62].

2.4. Mechanisms of Dye Adsorption

The enhanced performance of BC (without activation) can be due to oxygen containing surface functional groups and other inorganic components that play a significant role in dye adsorption instead of only surface area and porosity. BC inorganic elements upsurge the hydrophilicity towards dyes and act as catalysts during the adsorption process [63]. However, BC activation, surface area, and surface alkalinity can also influence adsorption capacity. Figure 3 represents the adsorption process and mechanism for dye removal from wastewater. Specific adsorption mechanisms include (i) physical adsorption, (ii) ion exchange; (iii) electrostatic interactions; (iv) precipitation; and (v) surface complexation [34,35]. However, the pollutant removal process always works in conjunction with numerous mechanisms.

2.4.1. Physical Adsorption

Dye adsorption onto the BC surface primarily occurs via physical interactions such as pore filling, π stacking, and H-bonding. However, BC surface area, porosity, and aromaticity influence the physical adsorption. The enhanced surface area and pore volume favor the diffusion of contaminants [64]. The aromatic structure of BC is promising for forming π -stacking and H-bond interactions with pollutants [65]. The pore filling, π - π interactions, and H bonding between BC and dye can be improved via post-modification of BC. For example, pore filling is an illustrative of physical adsorption and can be accredited to a widespread distribution of pores via BC [66]. Hydroxyl and amine groups can be an advantage for π - π interactions due to electron-deficient functional groups on the surface of cationic dyes [7]. For instance, cationic dyes H-bonding of O and/or N center generated free hydroxyl groups on the surface of sulfur-doped tapioca peel waste BC [67], whereas fly ash and agricultural waste-derived BC alkali-fusing with O-containing surface groups resulted in H-bonding [68]. The generation of H-bonds between acid orange 7 dye and the adsorbent accounts for the adsorption process [69]. Siddiqui et al. reported the H-bonds between methylene blue and MnO_2/BC occurs due to the interaction between the -OH groups present in MnO_2/BC and the acceptor present in the methylene blue molecules [70]. Likewise, π - π interactions/ π -effects/ π -interactions (non-covalent) involve the π system, where positively charged molecules interact with negatively charged surfaces, similar to electrostatic interactions [34].

2.4.2. Ion Exchange

Dye adsorption on the BC surface occurs via exchange of metal ions/mineral elements or replacement of BC functional groups [64]. Furthermore, the ion exchange mechanism involves ion exchange between a liquid (dye solution) and a solid phase (adsorbent). Pirbazari et al. suggested that two principal mechanisms are involved in the removal of methylene blue dye on NaOH-treated wheat straw impregnated with Fe_3O_4 , namely, surface complex formation and ion exchange between the dye molecules and adsorption

surfaces [71]. According to Zheng et al., the adsorption of anionic dyes such as Congo red and methyl orange on graphene oxide-NiFe layered double hydroxide is achieved by electrostatic attraction and ion exchange phenomena [72].

2.4.3. Electrostatic Attraction

Synthetic dyes are categorized into cationic and anionic dyes. Malachite green, methylene blue, and rhodamine B are examples of cationic dyes [73], and tartrazine, sunset yellow, Congo red, and orange G are examples of anionic dyes [74]. Knowledge of dye classification aid in choosing the accurate adsorbent as a positively charged adsorbent is effective in removing negatively charged dyes due to electrostatic interactions [74]. An electrostatic attraction occurs between the dye and BC surface when the surface charges are opposite [75]. Electrostatic interaction is one of the prime adsorption mechanisms for the adsorption of synthetic dyes on BC and can influence the adsorption rate. For instance, BC derived from litchi peel was assessed for adsorption of anionic and cationic dyes. The adsorption capacity was 404.4 and 2468 mg g⁻¹, respectively [45]. However, other adsorption mechanisms were also involved in the adsorption, and since the dye and BC both have opposite charges, the dye adsorption significantly occurred via electrostatic interactions [45]. Several BCs were designed for cationic and anionic dyes that fit either pseudo-second order or Elovich kinetic models, where both are indicative of electrostatic interactions and chemisorption. Shen and Gondal reported that electrostatic and intermolecular interactions govern the adsorption of rhodamine dye on adsorbent surfaces [76].

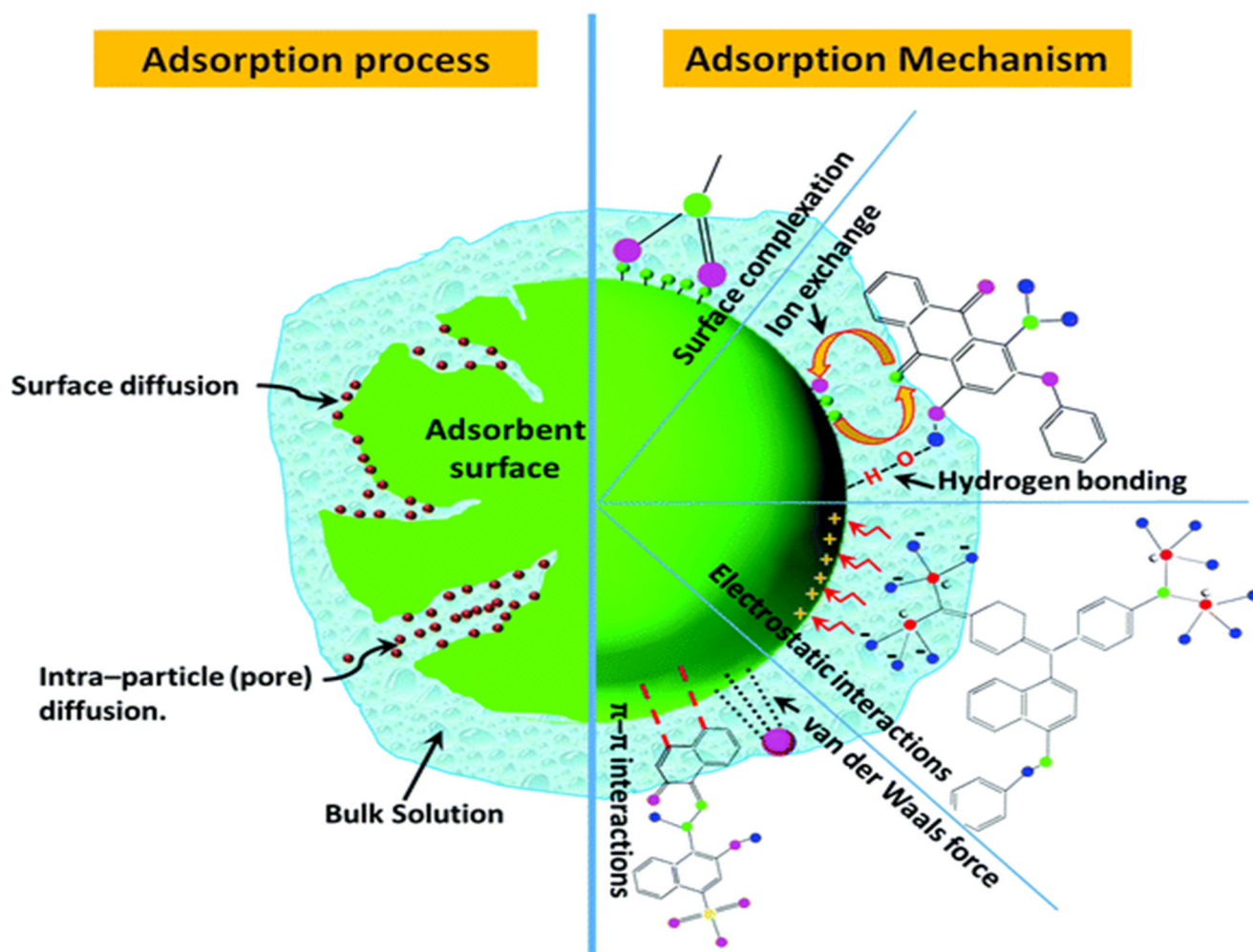


Figure 3. Adsorption process and mechanism for dye removal from wastewater [77].

3. Post-Production Modification of Biochar for Dye Removal

Biomass breaks down thermally in an oxygen-limited environment to generate BCs composed of numerous refractory oxides based on the feedstocks such as CaCO_3 , Fe_2O_3 , SiO_2 , Al_2O_3 , and CaSO_4 [78]. Moreover, pristine BC surfaces are generally negatively charged and linked with oxygen-bearing functional groups, thus displaying specific adsorption towards cations (e.g., heavy metals ions) [79]. However, adsorption of anionic species (i.e., oxyanion, anionic dyes, and organics) of BC is inadequate [80]. This restricts BC applications in various fields, instigating scientists to introduce novel metal oxides to alter BC for targeted applications [81]. Table 1 enlists few literatures available onto the treatment of dye-contaminated wastewater using BC and its nanocomposites. Table 1 enlist some literature available on the BC utilization for dye removal from wastewater.

Table 1. Literature summary on modified biochar for dye removal.

Synthetic Dye	Biochar		Adsorption Capacity	Conditions Adsorption Mechanism	Reference
	Feedstock	Method of Production			
Congo red	Litchi peel BC	Hydrothermal carbonization	404.4 mg g ⁻¹	Pore filling effect π - π interaction Electrostatic interaction Hydrogen bonding	[45]
	Orange peel waste	Microwave pyrolysis using CO ₂ and steam activation	136 mg g ⁻¹	Electrostatic interaction	[82]
	Switchgrass	Pyrolysis (900 °C)	22.6 mg g ⁻¹	Electrostatic interaction π - π interaction	[83]
Acid violet 17	Pine tree-derived BC	-	90%	Electrostatic interactions	[84]
Malachite green	Cladodes of cactus (<i>Opuntia ficus-indica</i>)	Pyrolysis at 400 °C followed by NaOH impregnation, pyrolysis at 500 °C and rinsing with HCl	1341 mg g ⁻¹	Π - π EDA interaction Cation- π interaction Hydrogen bonding	[85]
	Corn straw	HNO ₃ treatment, followed by washing with distilled water and drying. Then, NaOH activation and drying, followed by pyrolysis at 500 °C and FeCl ₃ modification by precipitation technique	515.8 mg g ⁻¹	Electrostatic attraction	[86]
	Frass of mealworms (<i>Tenebrio molitor</i> Linnaeus 1758)	Pyrolysis at 800 °C	1738.6 mg g ⁻¹	Electrostatic interaction π - π interaction Hydrogen bonding	[87]
	Litchi peel BC	Hydrothermal carbonization at 850 °C	2468 mg g ⁻¹	Pore filling effect π - π interaction Electrostatic interaction Hydrogen bonding	[45]
	Tapioca peel waste	Pyrolysis of feedstock, then mixing with thiourea and followed by pyrolysis at 800 °C to create sulfur-doped BC	30.2 mg g ⁻¹	Electrostatic interaction Hydrogen bonding	[67]
Methylene blue	Wakame (macroalgae)	Chemical activation with KOH followed by pyrolysis at 800 °C	4066.9 mg g ⁻¹	Electrostatic interaction π - π stacking Hydrogen bonding van der Waals force	[88]
	Macroalgae (<i>Undaria pinnatifida</i>)	Chemical activation with KOH followed by pyrolysis at 800 °C	841.6 mg g ⁻¹	Electrostatic interaction π - π interaction Hydrogen bonding and van der Waals force	[88]
	Rice straw and fly ash	Alkali-fusion pre-treatment of fly ash with NaOH, followed by mixing with rice straw and pyrolysis at 700 °C	143.8 mg g ⁻¹	Electrostatic interaction π - π interaction	[68]
Orange G	Switchgrass	Pyrolysis at 900 °C	38.2 mg g ⁻¹	Electrostatic interaction π - π interaction	[83]

Table 1. Cont.

Synthetic Dye	Biochar		Adsorption Capacity	Conditions Adsorption Mechanism	Reference
	Feedstock	Method of Production			
Rhodamine B	Macroalgae (<i>Undaria pinnatifida</i>)	Chemical activation with KOH followed by pyrolysis at 800 °C	533.8 mg g ⁻¹	Electrostatic interaction π-π interaction Hydrogen bonding van der Waals force	[88]
	Tapioca peel waste	Pyrolysis of feedstock, then mixing with thiourea and followed by pyrolysis at 800 °C to create sulfur-doped BC	33.1 mg g ⁻¹	Electrostatic interaction Hydrogen bonding	[67]
Sunset yellow/ Tartrazine	Corn cob	Pyrolysis at 400 °C followed by mixing with triethylenetetramine, drying and H ₂ SO ₄ treatment to achieve a positively charged BC	77.1 mg g ⁻¹	Amine groups on the surface Electrostatic interaction	[74]

Additionally, conventional pyrolysis generates BC with inefficient physicochemical properties such as surface area, surface-oxygenated groups, pore volume, and width. Different feedstock types have different BC production conditions and physicochemical properties [89]. However, the existing -COOH, -OH, and C=O functional groups are crucial in water treatment [90]. The hydrophilic or hydrophobic properties depend on the functional groups (nature and type) present on the BC surface. Various methods such as impregnation, steam activation, and chemical and heat treatments have been utilized to improve the abundant BC properties [91]. In the presence of other catalysts, BC acts as a photocatalyst due to the physicochemical properties (enhanced surface area, active site, charge separation, porous volume, functional groups, catalyzing ability, stability, and recoverability) [92]. However, photocatalyst-based BC production needs to be optimized [93]. For instance, the addition of ZnO to BC improves the nanocomposite adsorption capability and photocatalytic ability [94]. Figure 4 shows various modification and classification of engineered BC for the dye removal from wastewater.

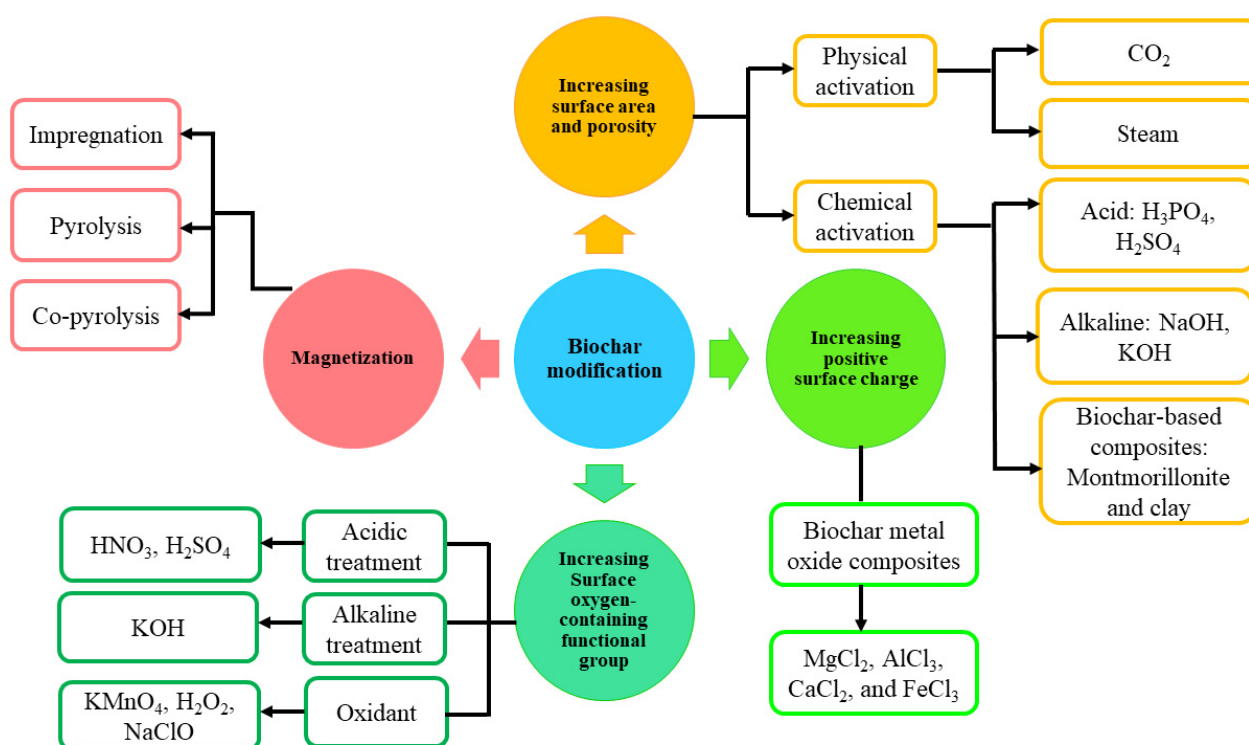


Figure 4. Modification and classification of engineered biochar.

Post-modification can be categorized into the following groups: (i) modifications to surge surface area and porosity; (ii) changes to decrease the positively charged BC surface; (iii) increase surface oxygen-containing functional groups; and (iv) magnetization of BC to enable recovery. Among all categories, any method can improve one or two BC properties simultaneously. For instance, the SSA and oxygen-containing functional groups can be increased by H_2SO_4 treatment. In the literature, these modifications are classified based on BC physicochemical characteristics or the nature of the process (chemical, physical, or composite) [95,96].

Furthermore, physical (van der Waals forces, electrostatic forces, and hydrophobic interactions) and chemical (surface complexation, ion exchange, π -interactions, co-precipitation, partition, and pore filling) interactions occur during adsorption of organic and inorganic pollutants by BC [97].

3.1. Acid-Base Activation/Decoration

Acid treatment of BC results in enhanced surface area, better porosity, increased sorption capacity, created charged and hydrophilic surface functional groups, and increased colloidal stability and mobility [98]. After BC oxidation, -OH and -COOH functional groups are enhanced to improve hydrophilicity. Acids such as $\text{HNO}_3/\text{H}_2\text{SO}_4$, HNO_3 , HF/HNO_3 , KMnO_4 , H_2O_2 , oxalic, and citric acids are used for chemical modification of BC [99].

One of the approaches for the modification of BC is HCl treatment resulting in higher adsorption of concomitant organic compounds. This is because functional groups (carboxylic, phenolic, and carbonyl groups) are added to the BC surface after treatment, the ash content is reduced, and the adsorption sites (hydrophobic) are increased [100,101]. However, this method is not well established for BC modification and more studies are needed to be performed [102].

The use of strong bases for BC modification increases functional groups, surface area, surface charge, and porosity [103]. However, the degree of improvement in BC properties varies depending on the base used. Frequently used bases include potassium oxide (KOH) and sodium hydroxide (NaOH) [104,105]. Few studies showed that the BC surface is significantly improved when using NaOH rather than KOH. For instance, Cazetta et al. [106] reported a better improvement in the surface area (49%) of coconut shell-derived BCs when using NaOH. Wakame-derived BC showed a surface area of $69.7 \text{ m}^2 \text{ g}^{-1}$ and $1156 \text{ m}^2 \text{ g}^{-1}$ for non-activated BC and KOH-activated BC, respectively [88]. Similarly, the BC surface area derived from rice husk improved from $132.9 \text{ m}^2 \text{ g}^{-1}$ for non-activated BC to $1818 \text{ m}^2 \text{ g}^{-1}$ for KOH-activated BC [107]. BC activation by KOH and KMnO_4 results in large pore volume, pore channels, and percentage of aromatized structures, enhancing the adsorption of methylene blue [108].

In general, modification of BC via acid is carried out in two ways: activation and decoration. BC activation via chemical activating agent increases SSA and porous structure. In contrast, decoration enhances the surface activity of BC via zero-valent iron nanoparticles [109], Fe_3O_4 , and FeOOH [110]. Studies have also shown that decoration using acids and fatty acids increases the hydrophobicity of BC adsorbents [111,112].

3.2. Persulfate Activation

Lately, the activation of BC via persulfate (PS) has been extensively studied [113] owing to the enhanced contaminant removal efficacy from water by the combination of PS radicals with BC-SSA [114]. Studies have shown that the sulfate radical-based advanced oxidation processes (AOP) have higher redox potentials, extended half-life time, and extensive pH flexibility than traditional hydroxyl radical-based AOP. Liu et al. [115] studied food waste digestate-derived BC (FWDB) for peroxydisulfate (PDS) catalyst (radical-based oxidant) for the removal of azo dye (reactive brilliant red X-3B). They observed a 92.21% removal of X-3B within 30 min from solution at an initial content of 1 g/L. The reactive oxygen species $\text{SO}_4^{\bullet-}$, $\bullet\text{OH}$, $\text{O}_2^{\bullet-}$, and $^1\text{O}_2$ were found to be present in the FWDB/PDS system and the generation of reactive oxygen species is due to the presence of graphitized carbon,

doped-N, oxygen-containing groups, and the defective sites on the FWDB surface. One-step sol-gel pyrolysis was used to synthesize CuFe₂O₄@BC composite (CuFe₂O₄@BC) and assessed for the efficiency, stability, and mechanism of activating PS against malachite green degradation [116]. The malachite green removal efficiency in the CuFe₂O₄@BC/PS system was observed to be 98.9%, signifying that CuFe₂O₄@BC has better catalytic activity compared to other catalysts under the optimal conditions.

A composite of stalk BC (SBC) and nanoscale zero-valent iron (nZVI) was biosynthesized to remove dye. The composite displayed a synergetic role in enhancing PS catalytic activity for dye removal [117]. SBC functional groups (-OH and -COOH) stimulated PS and nZVI improved catalytic activity compared to SBC. SBC enhances catalytic activity for PS and electron transfer efficiency by increasing nZVI dispersibility and protecting it from oxidation. Studies have shown that superoxide radicals (O₂^{•-}) and hydroxyl radicals (•OH) play an important part in pollutant removal, but they are not primary radicals. The primary radical involved in contaminant removal was sulfate radicals (SO₄^{•-}). The SBC-nZVI composite also displayed better reusability, storage stability, and various dye removal applications [117]. One-step pyrolysis of loofah sponge-based BC (LSB) was prepared at various pyrolytic temperatures. LSB was further used to activate PS to remove acid orange 7 (AO7) [118]. The LSB produced at 800 °C showed the best catalytic ability for AO7 degradation, i.e., 96% degradation within 30 min [118]. The enhanced adsorption capability of LSB is due to the high surface area, carbonyl groups, and graphitized structure. The AO7 degradation mechanism in the LSB-800/PS process is owing to free radical SO₄^{•-} and non-radical channels (electron transfer).

3.3. Physical Activation

In this process, different gases (air, steam, and CO₂) are used to activate the BC surface [119]. In general, physical activation consists of two stages: carbonization (occurs at lower temperatures of 427–877 °C) and activation (occurs at higher temperatures of 627–927 °C) [120]. BC activation can be carried out via steam or gas purging after BC is carbonized. Although this process is simple and cost-effective, it is less efficient than chemical activation approaches. BC physicochemical properties can be enhanced via physical activation by eliminating incomplete combustion by-products and the carbon surface oxidation to enhance BC surface area [121,122].

Pristine BC is activated by steam with improved polarity, surface area, and pore volume [123]. After preliminary pyrolysis, BC was partially vaporized by steam for 0.5 and 3 h [124]. Steam activation improves BC growth and the reachability of internal pores [124]. During steam activation, pore development is primarily associated with water-gas shift reaction, reduction of carbon [125], and elimination of trapped components (aldehydes, ketones, and some acids from biomass) [126].

In the presence of heated steam, BC is activated and displays high adsorption ability owing to improved surface area, oxygen-containing functional groups, and micropore volume. This allows for efficient removal of pollutants from wastewater [127]. The porosity of BC can be improved by physical activation at <250 °C in the presence of air or >750 °C in the presence of CO₂, steam, and blends. CO₂ and H₂O become reactive at high temperatures, allowing chemical reaction with BC [128]. CO₂ treatment increases the pore volume and surface area of BC by 1.5-fold and 5.9-fold, respectively [129]. At low temperatures (≈275 °C), the activation process with air increased the sewage sludge-derived BC structure and texture [130]. Furthermore, Sewu et al. [131] observed an increase in BC SSA and porosity via steam activation and significantly improved the crystal violet adsorption capacity by 4.1-fold.

3.4. Biochar-Based Composites

BC-based composites allow for the combined advantages of BC and nanomaterials, resulting in composites with enhanced functional groups, pore size and volume, active surface sites, net surface charge, ease of recovery, and catalytic ability for degradation [132,133].

These composites are divided into three groups according to the synthesis process: (i) nano-metal oxide/hydroxide-BC composites, (ii) magnetic BC composites [80], (iii) clay mineral-based BC [134].

3.4.1. Nano-Metal Oxide/Hydroxide-Biochar Composites

These composites have been synthesized via numerous chemical additives such as H_3PO_4 , $NaCl$, K_2CO_3 , $ZnCl_2$, KOH , and $FeCl_3$, and can be incorporated prior or later biomass carbonization [89]. According to Zhao et al. [135], the synthesis of nano-metal BC composites can be divided into the following categories: (i) impregnation, categorized by the ease and enormous capacity of the attained composites, (ii) chemical coprecipitation, categorized by inexpensiveness, high purity, homogeneous nanoparticles, but both process causes chemical contamination, (iii) direct pyrolysis, considered as easy process and biomass supplemented with desired heavy metals; however, controlling the nano-metal oxide/BC ratio in the composites is difficult, and (iv) ball milling, simple, cost-effective, no generation of chemical pollutants, and efficient decrease of metal oxide particle size. However, during particle preparation via ball milling, the particles are easily dispersed in water, resulting in the migration of contaminants out of the polluted place, causing a possible hazard to groundwater [135]. Figure 5 represents various pathways for synthesis of nano-metal oxide/hydroxide-BC composites.

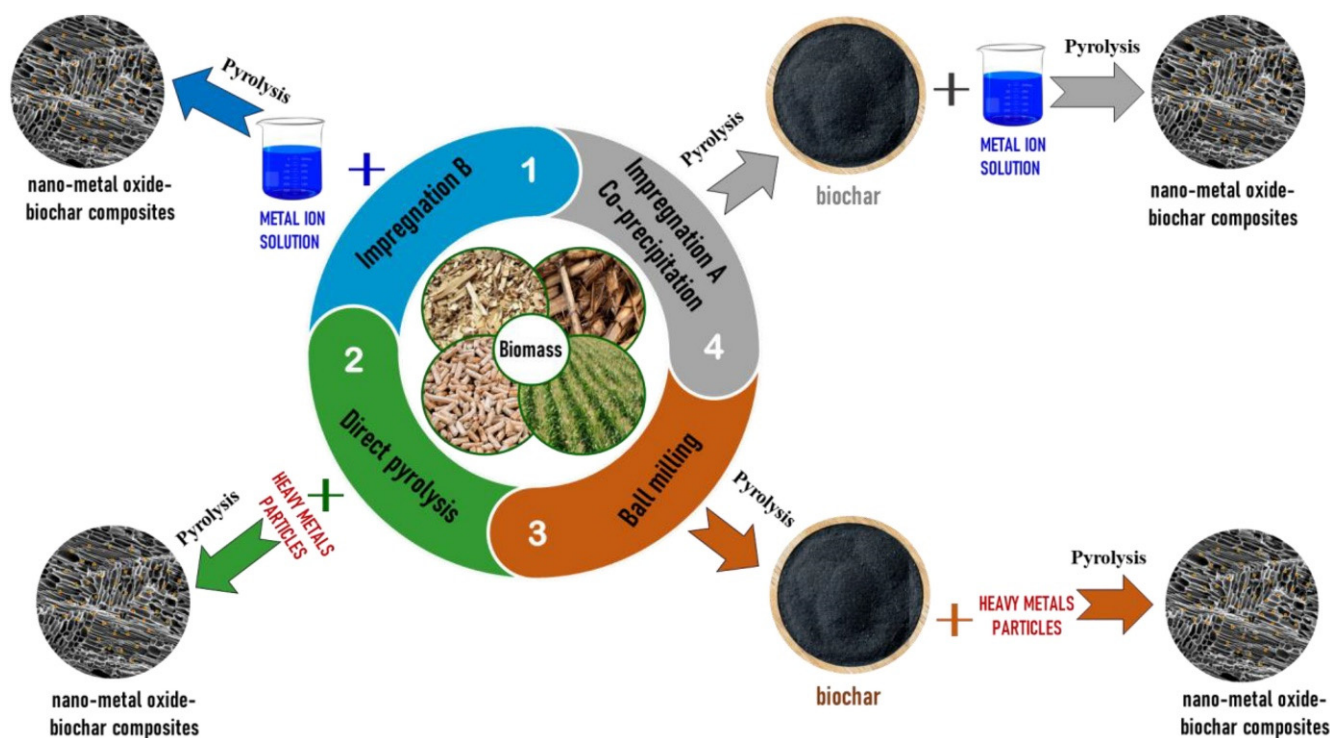


Figure 5. Various pathways for synthesis of nano-metal oxide/hydroxide-biochar composites. Reprinted with permission from [32].

Preparation of BC sample via ball milling surges SSA, possibly by revealing pores [136] and enhances carboxyl, lactone, and hydroxyl groups (oxygen-containing functional groups) [137]. Zheng et al. [138] synthesized a dual-function MgO/BC nanocomposite by ball milling to remove both cationic and anionic contaminants and showed an increased (8.4-fold) methylene blue adsorption, probably due to enhanced surface area and pore volume. Synthesis of BC by co-pyrolysis from firwood biomass utilizing non-magnetic goethite mineral proved to be a green method in comparison to the conventionally used $FeCl_3$ [139].

Sludge-derived BC was modified via Fe/Mn by a heterogeneous activator to attain enhanced PS activation to degrade reactive blue 19 (RB19) [140]. Experiments based on scavenger quenching and electron paramagnetic resonance displayed that radical and non-radical mechanisms are involved in the degradation of RB19 by Fe/MnBC combined PS. Sulfate radicals ($\text{SO}_4^{\bullet-}$), hydroxyl radicals (OH^{\bullet}), and singlet oxygen ($^1\text{O}_2$) were found to be involved in the process. It was also postulated that Fe(IV)/Mn(VII) (non-radical) was involved in the degradation process. These results provided a new understanding of the mechanism of PS activated by metal-BC composite. In addition, fixed-bed reactor studies revealed that Fe/MnBC has significant PS activation capability to remove dyes. Further, the authors analyzed degradation process by central composite design-response surface methodology (CCD-RSM) and ANN. Statistical analysis showed that the ANN model was better than the CCD-RSM model [140].

BC derived from pulp sludge was produced via ZnCl_2 modification to effectively remove methylene blue (MB) from aqueous solutions [141]. The maximum (590.20 mg/g) adsorption of MB was observed within 24 h at pH 8 when the initial amount of Zn^{2+} was 10 mg [141]. The primary mechanism involved in MB adsorption was electrostatic interaction between deprotonated functional groups and MB^+ , cation exchange, and π -electron interactions followed by physical adsorption.

3.4.2. Magnetized Biochar Composites

Substantial studies have been conducted to enhance BC adsorption capacity. However, the biggest limitation of BC is its removal and reuse after wastewater treatment owing to its small size and low density [59]. Various studies of magnetic BC for successful production have been reported [142], displaying impregnation-pyrolysis, chemical co-precipitation, solvothermal, and reductive co-precipitation processes. It was observed that the composites have a significantly efficient adsorption, easy removal and recycling after application of an external magnetic field [143]. However, the conventional magnetic medium loading process surges the sorbent cost [144]. The primary common processes of magnetic material synthesis include pyrolysis, co-precipitation, and calcination [145]. Figure 6 shows a brief schematic of different magnetic BC preparation.

Further, traditional heating in electric furnaces [146] and microwave heating in modified furnaces have also been studied. Among them, the co-precipitation method is easy because mixing and heating processes are simple. It emphasizes the transition metal ion molar ratios used in mixing to improve magnetic BC characteristics concerning porosity and magnetism [145]. The co-precipitation process is used for BC surface coating with various iron oxides such as Fe_3O_4 , $\alpha\text{-Fe}_2\text{O}_3$, and CoFe_2O_4 particles to impart magnetic characteristics to the iron oxide active sites for the pollutant removal [147,148]. It was observed that the high decomposition ability of additives such as AlCl_3 , FeCl_2 , and MgCl_2 displays enhanced porosity, high catalytic and sorption activity, and creation of positively charged adsorption sites [89,149].

Fe-tanned collagen fibers were pyrolyzed to synthesize magnetic BC catalyst (Fe@BC) utilized as a persulfate activator to remove a refractory dye (methylene blue) [150]. Results have shown that within 20 min, methylene blue was completely degraded at a constant rate of 0.2246 min^{-1} , much higher than when using pure BC (0.0497 min^{-1}). The enhanced catalytic activity and exceptional recycling ability of the Fe@BC/PS system can be attributed to the homogeneously dispersed Fe ions, enhanced functional groups (oxygen containing), and deformed carbon matrix. $\text{SO}_4^{\bullet-}$ was found to be the primary free radical for the degradation of methylene blue. Table 2 enlists literature on surface-modified BC and its nanocomposites for dye removal from wastewater.

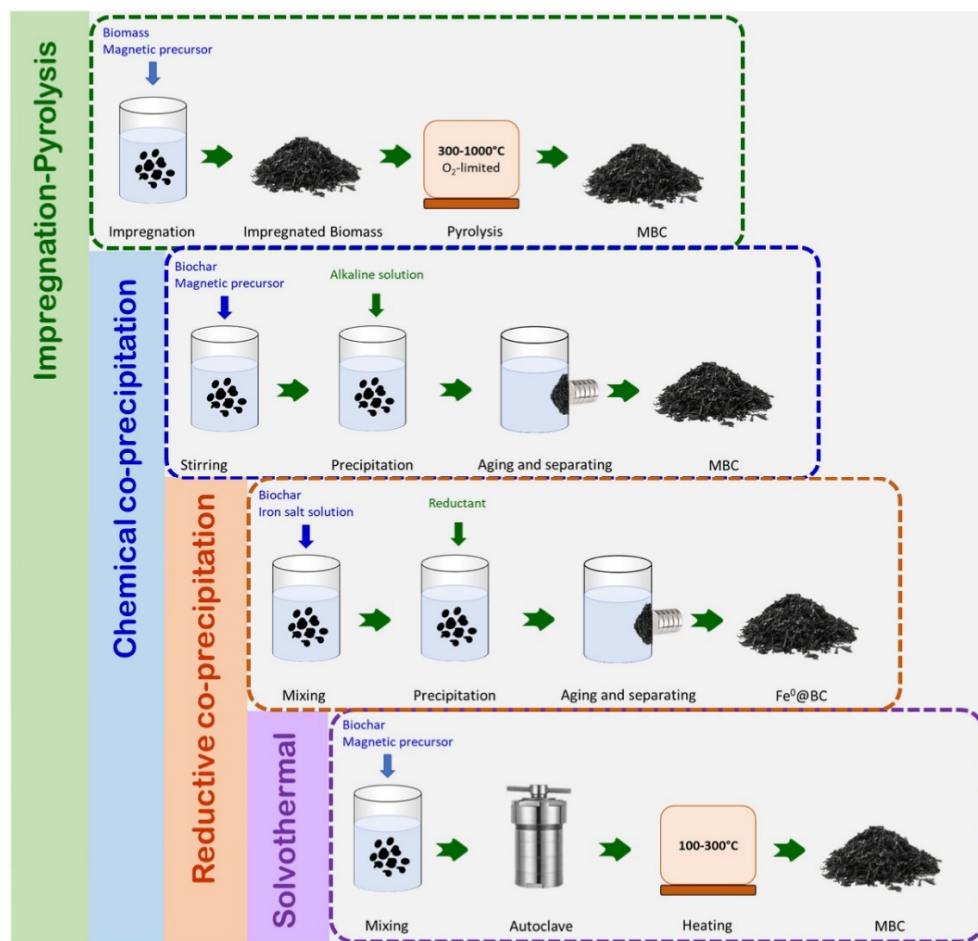


Figure 6. Brief schematic of different magnetic biochar preparation. Reprinted with permission from [32].

Table 2. Surface-modified biochar and its nanocomposites for dye removal from wastewater.

S. No.	Surface-Modified Biochar and Its Nanocomposites	Dye	Adsorption Model	Maximum Adsorption Capacity (mg/g)	Mechanism Involved	Reference
1.	TiO ₂ supported BC	3,4-dimethylaniline	Toth adsorption models	285.71	-	[151]
2.	Layered double-oxide/BC composites	Congo red	Langmuir	344.83	-	[152]
3.		Methyl orange	Langmuir	588.24	-	[152]
4.	CO ₂ and H ₂ O activator Pine sawdust BC	Methylene blue	Langmuir	160	Hydrogen bonding, ion exchange, π-π interaction	[153]
5.	Phosphomolybdate-modified BC	Methylene blue	Langmuir	146.23	Hydrogen bonding, electrostatic interactions, and ion exchange	[154]
6.	Banana peel BC/iron oxide composite	Methylene blue	Langmuir	862	-	[54]
7.	Mixed municipal discarded material derived BC	Methylene blue	Langmuir	7.2	π-π interactions	[155]
8.	KOH modified lychee seed BC	Methylene blue	Langmuir	124.5	-	[156]
9.	Triethylenetetramine corn cob BC	Sunset yellow	Langmuir	-	-	[74]
10.	Fe ₂ O ₃ /TiO ₂	Methylene blue	-	-	Reactive radical species	[157]
11.	functionalized wasted tea leaves derived BC	Rhodamine B	-	-		
12.		Methyl orange	-	-		

Table 2. Cont.

S. No.	Surface-Modified Biochar and Its Nanocomposites	Dye	Adsorption Model	Maximum Adsorption Capacity (mg/g)	Mechanism Involved	Reference
13.	Manganese-modified lignin BC	Methylene blue	Langmuir	248.96	-	[158]
14.	KOH activated pine BC	Methylene blue	Freundlich	637.5	Primary polar and π - π interactions	[109]
15.	KMnO ₄ activated pine BC	Methylene blue	Freundlich	439.5	Primary polar and π - π interactions	[109]
16.	Fe ₃ O ₄ -modified <i>Citrus bergamia</i> peel derived BC	Methylene blue	Langmuir	136.72	Electrostatic interaction	[26]
17.	Sulfuric acid modified BC from Pumpkin peel	Methylene Blue	Langmuir	208.3	-	[159]
18.	Acid activated Pine needle BC	Methylene blue	Langmuir	153.84	Hydrogen bonding, electrostatic interaction	[160]
19.	Laccase immobilized pine needle BC	Malachite green	-	-	Enzymatic degradation	[161]
20.	Ozonized saw dust BC	Methylene blue	Langmuir	200	Electrostatic interaction and hydrogen bonding	[162]
21.	Sonicated saw dust BC	Methylene blue	Langmuir	526		
22.	Nitric acid-treated <i>Pterospermum acerifolium</i> fruit waste BC	Methylene blue	Langmuir	-	-	[28]
23.	SDS-modified nitric acid-treated <i>Pterospermum acerifolium</i> fruit waste BC	Methylene blue	Langmuir	-	-	[28]
24.	Cetyl trimethyl ammonium bromide modified magnetic BC from pine nut shells	Acid chrome blue K	Langmuir	-	-	[27]

3.4.3. Modification via Clay Mineral

Pre-mixing of the feedstock prior to pyrolysis or post-mixing of the generated BC and clay minerals produces a clay-BC composite [95]. Arif et al. [134] studied the clay mineral-BC synthesis process and characteristics including pollutant interactions with the composite. This study displayed that clay-mineral amendment increases BC micropore area (>200%), whereas slight growth was detected in the mesopore area [163]. BC stability can also be enhanced by clay organo-mineral layers and avoid BC decomposition when applied to soil [164].

The interaction of the BC-clay/mineral composites with the pollutants involves various interactions such as ion exchange, precipitation, complexation, electrostatic interactions, hydrogen bonding, partitioning, electron-donor-acceptor interactions, hydrophobic interactions, and pore-filling [165]. Layered porous clay-BC (C-BC) was produced via layered bentonite clay intercalating properties comprising high cation exchange capacity with BC supporting redox-sensitive zero-valent iron (nZVI) nano-trident particles [166]. The synthesized C-BC-nZVI displayed a heterogeneous pore distribution on the C-BC-nZVI surface with dispersed un-oxidized nZVI particles (20–30 nm). Methylene blue was selectively adsorbed (52.1 mg/g) by nano-trident in the dye mixture. Further, pH and dissolved organic matter showed no influence on methylene blue sorption [166].

4. Application of Machine Learning and Artificial Neural Networks into Biochar-Facilitated Wastewater Remediation

The process initiates from BC production. Various techniques are then carried out to ensure the continued use of BC for wastewater treatment until it is landfilled or recycled. Precisely, the produced BCs are characterized as SSA, elemental composition and pH, used as input and aided in implementation [36]. Machine learning (ML) algorithms such as support vector regression, ANN, or random forests (RF) are applied at this stage. The data is processed via algorithm processes and the variables are transformed into files

using weights [167,168]. The decision criterion is made from the index to choose BC for wastewater treatment. After BC selection, it is passed on for wastewater treatment, where it is otherwise activated or functionalized by chemical or physical approaches. BC is re-characterized after activation/functionalization, and ML algorithms reprocess the data to determine whether the functionalized BC fulfils the standards required for wastewater treatment [36,169]. Moosavi et al. [170] compared the model performance of activated carbon derived from agricultural waste to remove dyes using gradient boosting, decision tree, and RF models. Model accuracy can be evaluated as correlation coefficient (R), mean squared error (MSE), and root mean squared error ($RMSE$) according to the following equations:

$$R = \sqrt{1 - \frac{\sum_{i=1}^N (\check{y}_i - y_i)^2}{\sum_{i=1}^N (\check{y}_i - \bar{y})^2}}, \quad (1)$$

$$MSE = \frac{1}{N} \sum_{i=1}^N (\check{y}_i - \bar{y})^2, \quad (2)$$

$$RMSE = \sqrt{MSE}. \quad (3)$$

The linear dependences amid any two variables or each attribute and the target variable are calculated by the following equation.

$$r_{xy} = \frac{\sum_{i=1}^n (x_i - \bar{x}) \sum_{i=1}^n (y_i - \bar{y})}{\sqrt{\sum_{i=1}^n (x_i - \bar{x})^2} \sqrt{\sum_{i=1}^n (y_i - \bar{y})^2}}, \quad (4)$$

where x or y is the mean of the factors x or y , respectively, and the data for each variable are normalized to a range of 0 and 1 using the equation below.

$$y = \frac{(x_i - x_{min})}{(x_{max} - x_{min})}, \quad (5)$$

where y is the normalized value of the initial x_i , and x_{max} and x_{min} are the maximum and minimum values of x_i , respectively.

Conventional modelling and optimization methods, i.e., RSM and statistical analysis, need a varied range of experiments, which are expensive and time consuming. Additionally, they do not precisely elucidate the association amid different factors affecting removal efficacy. ML is more robust and effective compared to statistical models when modelling complex data with possible nonlinearities or partial data [171]. ML offers stage for mapping associations amid input and output parameters during pollutant remediation. It is grounded on computer algorithms that are automatically developed and adjusted to specified conditions, with the ability to forecast the properties of concern via the knowledge and interpretation carried out by machines. It is used to study complex associations amid adsorbent properties (e.g., surface area, total pore volume, average pore diameter, and elemental composition), adsorption conditions, and adsorption performance without empirical assumptions [172]. Moreover, the foremost goal of system modelling and simulation is to obtain data on the progress of the system without conducting experiments. Thus, it is essential to develop a multidimensional nature model that can adapt to each process. Regarding the problem of overlooking variable relationships, ML models have demonstrated beneficial tools for method design, regression models, and response optimization [173].

Non-linear associations between independent and dependent variables can be created by ANN models grounded on a set of test results. Recently, the use of ANN models for modelling dye adsorption has become very common. Based on the ANN model type, dye adsorption can be categorized into the following groups: (i) multilayer feedforward neural networks, (ii) adaptive neuro-fuzzy inference systems, (iii) support vector regression, and (iv) hybrid models. Various ANN models were used to assess dye removal [174]. A three-layer feedforward backpropagation network (FFBPN) was used to study the removal of acid orange from an aqueous medium by powdered activated carbon [175]. In an input

layer with three neurons (consisting of initial pH, dye concentration, and contact time) and an output layer with one neuron (dye concentration after time 't'), they established FFBPN. As a result of evaluating the model's performance using the mean relative error (MRE), it was found to be 5.81%. This MRE value signifies that the ANN model had good analytical performance and can be used in place of kinetic studies.

5. Conclusions and Future Perspectives

BC has been considered an efficient adsorbent to treat wastewater owing to the presence of abundant functional groups and large surface area. Few studies assessed expenses during the production of BC-based adsorbents. A cost-effective technique and the reuse of multiple cycles are possible. However, additional investigation of numerous outlooks is obligatory to confirm BC efficiency and inexpensiveness, mainly for pilot-scale implementation in subsequent fields.

- (1) To attain optimum BC efficacy, it is crucial to study the relations amid various parameters, such as production process, modification/functionalization, and handling all in an eco-friendly way.
- (2) Moreover, promising sorbents that are effectively suitable for pilot scale must be inexpensive and resources ought to be widely accessible in huge amounts in nature. Recycling of sorbents on a large scale can reduce costs and energy consumption to provide sustainable products.
- (3) Involvement of software to optimize factors affecting pollutant removal by BC is an innovative and powerful tool in experimental design and analysis. Applications of ANN and ML can be used to predict and reduce explicit computer programming.

Modified clay/BC composites displayed significant benefits compared to modified clays alone, owing to their cost-effective, high adsorption ability, and anionic dye removal effect. However, few studies have been carried out on a pilot scale. The advancement of magnetic BC research with organic pollutant removal is a vital and new research area, and more research in this field should be conducted in the future. However, generation of noxious components during the synthesis of magnetic BC should be careful.

BC delivers a robust interaction between the BC surface and various pollutants existing in water and soil. However, as BC loaded with pollutants may pose serious hazard associated with disposal, a new challenge for researchers concerning the prospects for the transformed environmental movement of these pollutants is to change the context of pollutant hazard valuation in the milieu. Implementation of a sustainable management strategy for contaminant loaded-BC is life threatening. This approach should follow the concept of a circular economy and should allow for an eco-friendly and cost-effective recycling of these BCs in the forthcoming adsorption cycles. In addition, during laboratory scale studies, knowledge of the mechanisms of chemical and physical interaction of BC with pollutants is required. Promising technologies always have a secondary hazard, and the utilization of BC loaded with pollutant for bio-oil production in the future could be a fascinating area that must be explored.

ANN and ML predictive models reduce workload, budget, space requirements, and pollutant remediation time. For instance, ML can be used to develop models to improve pyrolysis process and forecast the yield of BC depending on raw material characteristics and process conditions, which can help develop a sustainable wastewater treatment system. Further, the commencement of more compacted reactors capable of accommodating BC-supported catalysts are required for implementation. Future research should be devoted to the application of BC-based catalysts in large-scale reactors, which can be implemented at the industrial level. It is urgent to further explore the potential of BC in real challenging systems.

Author Contributions: L.G.: writing—original draft preparation; A.K.: writing—review and editing; S.R.K.: writing—review and editing; B.-S.K.: writing—review and editing. All authors have read and agreed to the published version of the manuscript.

Funding: This research was supported by National Research Foundation of Korea (NRF-2019R111A-3A02058523).

Data Availability Statement: The study did not report any data.

Conflicts of Interest: There are no financial conflict of interest to disclose.

References

1. Bouckaert, S.; Pales, A.F.; McGlade, C.; Remme, U.; Wanner, B.; Varro, L.; Spencer, T. *Net Zero by 2050: A Roadmap for the Global Energy Sector*; International Energy Agency: Paris, France, 2021.
2. Sathe, S.S.; Goswami, L.; Mahanta, C. Arsenic reduction and mobilization cycle via microbial activities prevailing in the Holocene aquifers of Brahmaputra flood plain. *Groundw. Sustain. Dev.* **2021**, *13*, 100578. [[CrossRef](#)]
3. Kushwaha, A.; Goswami, S.; Hans, N.; Goswami, L.; Devi, G.; Deshavath, N.N.; Lall, A.M. An insight into biological and chemical technologies for micropollutant removal from wastewater. In *Fate and Transport of Subsurface Pollutants*; Springer: Singapore, 2021; pp. 199–226.
4. Mallakpour, S.; Lormahdiabadi, M. Removal of the Anionic Dye Congo Red from an Aqueous Solution Using a Crosslinked Poly (vinyl alcohol)-ZnO-Vitamin M Nanocomposite Film: A Study of the Recent Concerns about Nonlinear and Linear Forms of Isotherms and Kinetics. *Langmuir* **2022**, *38*, 4065–4076. [[CrossRef](#)] [[PubMed](#)]
5. Hussain, C.M.; Singh, S.; Goswami, L. *Emerging Trends to Approaching Zero Waste*; Elsevier: Amsterdam, The Netherlands, 2021.
6. Hussain, C.M.; Singh, S.; Goswami, L. (Eds.) *Waste-to-Energy Approaches towards Zero Waste: Interdisciplinary Methods of Controlling Waste*; Elsevier: Amsterdam, The Netherlands, 2021.
7. Choudhary, M.; Kumar, R.; Neogi, S. Activated biochar derived from *Opuntia ficus-indica* for the efficient adsorption of malachite green dye, Cu^{+2} and Ni^{+2} from water. *J. Hazard. Mater.* **2020**, *392*, 122441. [[CrossRef](#)]
8. Begum, W.; Goswami, L.; Sharma, B.B.; Kushwaha, A. Assessment of urban river pollution using the water quality index and macro-invertebrate community index. *Environ. Dev. Sustain.* **2022**, 1–26. [[CrossRef](#)]
9. Goswami, S.; Kushwaha, A.; Goswami, L.; Singh, N.; Bhan, U.; Daverey, A.; Hussain, C.M. Biological treatment, recovery, and recycling of metals from waste printed circuit boards. In *Environmental Management of Waste Electrical and Electronic Equipment*; Elsevier: Amsterdam, The Netherlands, 2021; pp. 163–184.
10. Lata, K.; Kushwaha, A.; Ramanathan, G. Bacterial enzymatic degradation and remediation of 2,4,6-trinitrotoluene. *Microb. Nat. Macromol.* **2021**, *23*, 623–659.
11. Vadivel, V.K.; Cikurel, H.; Mamane, H. Removal of Indigo Dye by $\text{CaCO}_3/\text{Ca}(\text{OH})_2$ Composites and Resource Recovery. *Ind. Eng. Chem. Res.* **2021**, *60*, 10312–10318. [[CrossRef](#)]
12. Kumar, M.; Kushwaha, A.; Goswami, L.; Singh, A.K.; Sikandar, M. A review on advances and mechanism for the phycoremediation of cadmium contaminated wastewater. *Clean. Eng. Technol.* **2021**, *5*, 100288. [[CrossRef](#)]
13. Rizvi, S.; Singh, A.; Kushwaha, A.; Gupta, S.K. Recent advances in melanoidin removal from wastewater: Sources, properties, toxicity, and remediation strategies. In *Emerging Trends to Approaching Zero Waste*; Elsevier: Amsterdam, The Netherlands, 2022; pp. 361–386.
14. Patra, D.; Patra, B.R.; Pattnaik, F.; Hans, N.; Kushwaha, A. Recent evolution in green technologies for effective valorization of food and agricultural wastes. In *Emerging Trends to Approaching Zero Waste*; Elsevier: Amsterdam, The Netherlands, 2022; pp. 103–132.
15. Kushwaha, A.; Goswami, S.; Hans, N.; Singh, A.; Vishwakarma, H.S.; Devi, G.; Hussain, C.M. Sorption of pharmaceutical and personal care products from the wastewater by carbonaceous materials. In *Emerging Trends to Approaching Zero Waste*; Elsevier: Amsterdam, The Netherlands, 2021; pp. 175–196.
16. Saha, P.; Goswami, L.; Kim, B.S. Novel Biobased Non-Isocyanate Polyurethanes from Microbially Produced 7,10-Dihydroxy-8 (E)-Octadecenoic Acid for Potential Packaging and Coating Applications. *ACS Sustain. Chem. Eng.* **2022**, *10*, 4623–4633. [[CrossRef](#)]
17. Ojaswini, C.; Sathe, S.S.; Mahanta, C.; Kushwaha, A. Evaluation of iron coated natural sand for removal of dissolved arsenic from groundwater and develop sustainable filter media. *Environ. Nanotechnol. Monit. Manag.* **2022**, *18*, 100682. [[CrossRef](#)]
18. Gautam, A.; Kushwaha, A.; Rani, R. Microbial remediation of hexavalent chromium: An eco-friendly strategy for the remediation of chromium-contaminated wastewater. In *The Future of Effluent Treatment Plants*; Elsevier: Amsterdam, The Netherlands, 2021; pp. 361–384.
19. Gupt, C.B.; Kushwaha, A.; Prakash, A.; Chandra, A.; Goswami, L.; Sekharan, S. Mitigation of groundwater pollution: Heavy metal retention characteristics of fly ash based liner materials. In *Fate and Transport of Subsurface Pollutants*; Springer: Singapore, 2021; pp. 79–104.
20. Kushwaha, A.; Rani, R.; Patra, J.K. Adsorption kinetics and molecular interactions of lead [Pb (II)] with natural clay and humic acid. *Int. J. Environ. Sci. Technol.* **2020**, *17*, 1325–1336. [[CrossRef](#)]

21. Goswami, L.; Manikandan, N.A.; Taube, J.C.R.; Pakshirajan, K.; Pugazhenthii, G. Novel waste-derived biochar from biomass gasification effluent: Preparation, characterization, cost estimation, and application in polycyclic aromatic hydrocarbon biodegradation and lipid accumulation by *Rhodococcus opacus*. *Environ. Sci. Pollut. Res.* **2019**, *26*, 25154–25166. [[CrossRef](#)]
22. Goswami, L.; Kushwaha, A.; Singh, A.; Saha, P.; Choi, Y.; Maharana, M.; Kim, B.S. Nano-biochar as a sustainable catalyst for anaerobic digestion: A synergetic closed-loop approach. *Catalysts* **2022**, *12*, 186. [[CrossRef](#)]
23. Goswami, S.; Kushwaha, A.; Goswami, L.; Gupta, N.R.; Kumar, V.; Bhan, U.; Tripathi, K.M. Nanobiochar-a green catalyst for wastewater remediation. In *Bio-Based Nanomaterials*; Elsevier: Amsterdam, The Netherlands, 2022; pp. 109–132.
24. Goswami, L.; Pakshirajan, K.; Pugazhenthii, G. Biological treatment of biomass gasification wastewater using hydrocarbonoclastic bacterium *Rhodococcus opacus* in an up-flow packed bed bioreactor with a novel waste-derived nano-biochar based bio-support material. *J. Clean. Prod.* **2020**, *256*, 120253. [[CrossRef](#)]
25. Salleh, M.A.M.; Mahmoud, D.K.; Karim, W.A.W.A.; Idris, A. Cationic and anionic dye adsorption by agricultural solid wastes: A comprehensive review. *Desalination* **2011**, *280*, 1–13. [[CrossRef](#)]
26. Tripathy, S.; Sahu, S.; Patel, R.K.; Panda, R.B.; Kar, P.K. Novel Fe₃O₄-Modified Biochar Derived from Citrus Bergamia Peel: A Green Synthesis Approach for Adsorptive Removal of Methylene Blue. *ChemistrySelect* **2022**, *7*, e202103595. [[CrossRef](#)]
27. Wang, H.; Wang, S.; Gao, Y. Cetyl trimethyl ammonium bromide modified magnetic biochar from pine nut shells for efficient removal of acid chrome blue K. *Bioresour. Technol.* **2020**, *312*, 123564. [[CrossRef](#)]
28. Oraon, A.; Prajapati, A.K.; Ram, M.; Saxena, V.K.; Dutta, S. Synthesis, characterization, and application of microporous biochar prepared from *Pterospermum acerifolium* plant fruit shell waste for methylene blue dye adsorption: The role of surface modification by SDS surfactant. *Biomass Convers. Biorefin.* **2022**, 1–23. [[CrossRef](#)]
29. Al-Rumaihi, A.; Shahbaz, M.; McKay, G.; Mackey, H.; Al-Ansari, T. A review of pyrolysis technologies and feedstock: A blending approach for plastic and biomass towards optimum biochar yield. *Renew. Sustain. Energy Rev.* **2022**, *167*, 112715. [[CrossRef](#)]
30. Zaman, C.Z.; Pal, K.; Yehye, W.A.; Sagadevan, S.; Shah, S.T.; Adebisi, G.A.; Johan, R.B. *Pyrolysis: A Sustainable Way to Generate Energy from Waste*; IntechOpen: Rijeka, Croatia, 2017; Volume 1, p. 316806.
31. Liu, W.J.; Jiang, H.; Yu, H.Q. Development of biochar-based functional materials: Toward a sustainable platform carbon material. *Chem. Rev.* **2015**, *115*, 12251–12285. [[CrossRef](#)] [[PubMed](#)]
32. Zeghioud, H.; Fryda, L.; Djelal, H.; Assadi, A.; Kane, A. A comprehensive review of biochar in removal of organic pollutants from wastewater: Characterization, toxicity, activation/functionalization and influencing treatment factors. *J. Water Process Eng.* **2022**, *47*, 102801. [[CrossRef](#)]
33. Tripathi, M.; Sahu, J.N.; Ganesan, P. Effect of process parameters on production of biochar from biomass waste through pyrolysis: A review. *Renew. Sustain. Energy Rev.* **2016**, *55*, 467–481. [[CrossRef](#)]
34. Yaashikaa, P.R.; Kumar, P.S.; Varjani, S.; Saravanan, A. A critical review on the biochar production techniques, characterization, stability and applications for circular bioeconomy. *Biotechnol. Rep.* **2020**, *28*, e00570. [[CrossRef](#)]
35. Liu, Y.; Chen, Y.; Li, Y.; Chen, L.; Jiang, H.; Li, H.; Hou, S. Fabrication, application, and mechanism of metal and heteroatom co-doped biochar composites (MHBCs) for the removal of contaminants in water: A review. *J. Hazard. Mater.* **2022**, *431*, 128584. [[CrossRef](#)]
36. Da Silva Medeiros, D.C.C.; Nzediegwu, C.; Benally, C.; Messele, S.A.; Kwak, J.H.; Naeth, M.A.; El-Din, M.G. Pristine and engineered biochar for the removal of contaminants co-existing in several types of industrial wastewaters: A critical review. *Sci. Total Environ.* **2021**, *809*, 151120. [[CrossRef](#)]
37. Das, O.; Bhattacharyya, D.; Hui, D.; Lau, K.T. Mechanical and flammability characterisations of biochar/polypropylene biocomposites. *Compos. Part B Eng.* **2016**, *106*, 120–128. [[CrossRef](#)]
38. Zou, H.; Zhao, J.; He, F.; Zhong, Z.; Huang, J.; Zheng, Y.; Gao, B. Ball milling biochar iron oxide composites for the removal of chromium (Cr (VI)) from water: Performance and mechanisms. *J. Hazard. Mater.* **2021**, *413*, 125252. [[CrossRef](#)]
39. Li, S.; Harris, S.; Anandhi, A.; Chen, G. Predicting biochar properties and functions based on feedstock and pyrolysis temperature: A review and data syntheses. *J. Clean. Prod.* **2019**, *215*, 890–902. [[CrossRef](#)]
40. Agrafioti, E.; Bouras, G.; Kalderis, D.; Diamadopoulos, E. Biochar production by sewage sludge pyrolysis. *J. Anal. Appl. Pyrolysis* **2013**, *101*, 72–78. [[CrossRef](#)]
41. Amonette, J.E.; Joseph, S. Characteristics of biochar: Microchemical properties. In *Biochar for Environmental Management*; Routledge: London, UK, 2012; pp. 65–84.
42. Huang, Q.; Song, S.; Chen, Z.; Hu, B.; Chen, J.; Wang, X. Biochar-based materials and their applications in removal of organic contaminants from wastewater: State-of-the-art review. *Biochar* **2019**, *1*, 45–73. [[CrossRef](#)]
43. Tan, X.; Liu, Y.; Zeng, G.; Wang, X.; Hu, X.; Gu, Y.; Yang, Z. Application of biochar for the removal of pollutants from aqueous solutions. *Chemosphere* **2015**, *125*, 70–85. [[CrossRef](#)] [[PubMed](#)]
44. Ambaye, T.G.; Vaccari, M.; van Hullebusch, E.D.; Amrane, A.; Rtimi, S. Mechanisms and adsorption capacities of biochar for the removal of organic and inorganic pollutants from industrial wastewater. *Int. J. Environ. Sci. Technol.* **2021**, *18*, 3273–3294. [[CrossRef](#)]
45. Wu, J.; Yang, J.; Feng, P.; Huang, G.; Xu, C.; Lin, B. High-efficiency removal of dyes from wastewater by fully recycling litchi peel biochar. *Chemosphere* **2020**, *246*, 125734. [[CrossRef](#)] [[PubMed](#)]
46. Qambrani, N.A.; Rahman, M.M.; Won, S.; Shim, S.; Ra, C. Biochar properties and eco-friendly applications for climate change mitigation, waste management, and wastewater treatment: A review. *Renew. Sustain. Energy Rev.* **2017**, *79*, 255–273. [[CrossRef](#)]

47. Kushwaha, A.; Rani, R.; Kumar, S.; Thomas, T.; David, A.A.; Ahmed, M. A new insight to adsorption and accumulation of high lead concentration by copolymer and whole cells of lead-resistant bacterium *Acinetobacter junii* L. Pb1 isolated from coal mine dump. *Environ. Sci. Pollut. Res.* **2017**, *24*, 10652–10661. [[CrossRef](#)] [[PubMed](#)]
48. Enaime, G.; Baçaoui, A.; Yaacoubi, A.; Lübken, M. Biochar for wastewater treatment-conversion technologies and applications. *Appl. Sci.* **2020**, *10*, 3492. [[CrossRef](#)]
49. Gautam, R.K.; Goswami, M.; Mishra, R.K.; Chaturvedi, P.; Awashthi, M.K.; Singh, R.S.; Pandey, A. Biochar for remediation of agrochemicals and synthetic organic dyes from environmental samples: A review. *Chemosphere* **2021**, *272*, 129917. [[CrossRef](#)]
50. Qiu, Y.; Zheng, Z.; Zhou, Z.; Sheng, G.D. Effectiveness and mechanisms of dye adsorption on a straw-based biochar. *Bioresour. Technol.* **2009**, *100*, 5348–5351. [[CrossRef](#)] [[PubMed](#)]
51. Kaya, N.; Yıldız, Z.; Ceylan, S. Preparation and characterisation of biochar from hazelnut shell and its adsorption properties for methylene blue dye. *Politek. Derg.* **2018**, *21*, 765–776. [[CrossRef](#)]
52. Lin, Y.C.; Ho, S.H.; Zhou, Y.; Ren, N.Q. Highly efficient adsorption of dyes by biochar derived from pigments-extracted macroalgae pyrolyzed at different temperature. *Bioresour. Technol.* **2018**, *259*, 104–110.
53. Nautiyal, P.; Subramanian, K.A.; Dastidar, M.G. Adsorptive removal of dye using biochar derived from residual algae after in-situ transesterification: Alternate use of waste of biodiesel industry. *J. Environ. Manag.* **2016**, *182*, 187–197. [[CrossRef](#)] [[PubMed](#)]
54. Zhang, P.; O'Connor, D.; Wang, Y.; Jiang, L.; Xia, T.; Wang, L.; Hou, D. A green biochar/iron oxide composite for methylene blue removal. *J. Hazard. Mater.* **2020**, *384*, 121286. [[CrossRef](#)] [[PubMed](#)]
55. Chowdhury, S.; Chakraborty, S.; Saha, P. Biosorption of Basic Green 4 from aqueous solution by *Ananas comosus* (pineapple) leaf powder. *Colloids Surf. B Biointerfaces* **2011**, *84*, 520–527. [[CrossRef](#)]
56. Dawood, S.; Sen, T.K.; Phan, C. Adsorption removal of Methylene Blue (MB) dye from aqueous solution by bio-char prepared from *Eucalyptus sheathiana* bark: Kinetic, equilibrium, mechanism, thermodynamic and process design. *Desalination Water Treat.* **2016**, *57*, 28964–28980. [[CrossRef](#)]
57. Biswas, S.; Mohapatra, S.S.; Kumari, U.; Meikap, B.C.; Sen, T.K. Batch and continuous closed circuit semi-fluidized bed operation: Removal of MB dye using sugarcane bagasse biochar and alginate composite adsorbents. *J. Environ. Chem. Eng.* **2020**, *8*, 103637. [[CrossRef](#)]
58. Xu, Y.; Chen, B. Investigation of thermodynamic parameters in the pyrolysis conversion of biomass and manure to biochars using thermogravimetric analysis. *Bioresour. Technol.* **2013**, *146*, 485–493. [[CrossRef](#)]
59. Li, C.; Hayashi, J.I.; Sun, Y.; Zhang, L.; Zhang, S.; Wang, S.; Hu, X. Impact of heating rates on the evolution of function groups of the biochar from lignin pyrolysis. *J. Anal. Appl. Pyrolysis* **2021**, *155*, 105031. [[CrossRef](#)]
60. Yorgun, S.; Yıldız, D.; Şimşek, Y.E. Activated carbon from paulownia wood: Yields of chemical activation stages. *Energy Sources Part A Recovery Util. Environ. Eff.* **2016**, *38*, 2035–2042. [[CrossRef](#)]
61. Harun, N.Y.; Afzal, M.T. Effect of particle size on mechanical properties of pellets made from biomass blends. *Procedia Eng.* **2016**, *148*, 93–99. [[CrossRef](#)]
62. Bourke, J.; Manley-Harris, M.; Fushimi, C.; Dowaki, K.; Nunoura, T.; Antal, M.J. Do all carbonized charcoals have the same chemical structure? 2. A model of the chemical structure of carbonized charcoal. *Ind. Eng. Chem. Res.* **2007**, *46*, 5954–5967. [[CrossRef](#)]
63. Alias, N.; Zaini, M.A.A.; Kamaruddin, M.J. Roles of impregnation ratio of K_2CO_3 and NaOH in chemical activation of palm kernel shell. *J. Appl. Sci. Process Eng.* **2017**, *4*, 195–204. [[CrossRef](#)]
64. Inyang, M.I.; Gao, B.; Yao, Y.; Xue, Y.; Zimmerman, A.; Mosa, A.; Cao, X. A review of biochar as a low-cost adsorbent for aqueous heavy metal removal. *Crit. Rev. Environ. Sci. Technol.* **2016**, *46*, 406–433. [[CrossRef](#)]
65. Ma, J.; Zhou, B.; Zhang, H.; Zhang, W. Fe/S modified sludge-based biochar for tetracycline removal from water. *Powder Technol.* **2020**, *364*, 889–900. [[CrossRef](#)]
66. Wu, M.; Wang, Y.; Lu, B.; Xiao, B.; Chen, R.; Liu, H. Efficient activation of peroxydisulfate and degradation of Orange G in iron phosphide prepared by pickling waste liquor. *Chemosphere* **2021**, *269*, 129398. [[CrossRef](#)]
67. Vigneshwaran, S.; Sirajudheen, P.; Karthikeyan, P.; Meenakshi, S. Fabrication of sulfur-doped biochar derived from tapioca peel waste with superior adsorption performance for the removal of Malachite green and Rhodamine B dyes. *Surf. Interfaces* **2021**, *23*, 100920. [[CrossRef](#)]
68. Wang, K.; Peng, N.; Sun, J.; Lu, G.; Chen, M.; Deng, F.; Zhong, Y. Synthesis of silica-composited biochars from alkali-fused fly ash and agricultural wastes for enhanced adsorption of methylene blue. *Sci. Total Environ.* **2020**, *729*, 139055. [[CrossRef](#)]
69. Cojocar, C.; Samoila, P.; Pascariu, P. Chitosan-based magnetic adsorbent for removal of water-soluble anionic dye: Artificial neural network modeling and molecular docking insights. *Int. J. Biol. Macromol.* **2019**, *123*, 587–599. [[CrossRef](#)]
70. Siddiqui, S.I.; Manzoor, O.; Mohsin, M.; Chaudhry, S.A. *Nigella sativa* seed-based nanocomposite-MnO₂/BC: An antibacterial material for photocatalytic degradation, and adsorptive removal of Methylene blue from water. *Environ. Res.* **2019**, *171*, 328–340. [[CrossRef](#)]
71. Pirbazari, A.E.; Saberikhah, E.; Kozani, S.H. Fe₃O₄-wheat straw: Preparation, characterization and its application for methylene blue adsorption. *Water Resour. Ind.* **2014**, *7*, 23–37. [[CrossRef](#)]
72. Zheng, Y.; Cheng, B.; You, W.; Yu, J.; Ho, W. 3D hierarchical graphene oxide-NiFe LDH composite with enhanced adsorption affinity to Congo red, methyl orange and Cr (VI) ions. *J. Hazard. Mater.* **2019**, *369*, 214–225. [[CrossRef](#)] [[PubMed](#)]

73. Li, H.; Cao, X.; Zhang, C.; Yu, Q.; Zhao, Z.; Niu, X.; Li, Z. Enhanced adsorptive removal of anionic and cationic dyes from single or mixed dye solutions using MOF PCN-222. *RSC Adv.* **2017**, *7*, 16273–16281. [[CrossRef](#)]
74. Mahmoud, M.E.; Abdelfattah, A.M.; Tharwat, R.M.; Nabil, G.M. Adsorption of negatively charged food tartrazine and sunset yellow dyes onto positively charged triethylenetetramine biochar: Optimization, kinetics and thermodynamic study. *J. Mol. Liq.* **2020**, *318*, 114297. [[CrossRef](#)]
75. Ho, S.H.; Zhu, S.; Chang, J.S. Recent advances in nanoscale-metal assisted biochar derived from waste biomass used for heavy metals removal. *Bioresour. Technol.* **2017**, *246*, 123–134. [[CrossRef](#)]
76. Shen, K.; Gondal, M.A. Removal of hazardous Rhodamine dye from water by adsorption onto exhausted coffee ground. *J. Saudi Chem. Soc.* **2017**, *21*, S120–S127. [[CrossRef](#)]
77. Dutta, S.; Gupta, B.; Srivastava, S.K.; Gupta, A.K. Recent advances on the removal of dyes from wastewater using various adsorbents: A critical review. *Mater. Adv.* **2021**, *2*, 4497–4531. [[CrossRef](#)]
78. Vijayaraghavan, K. The importance of mineral ingredients in biochar production, properties and applications. *Crit. Rev. Environ. Sci. Technol.* **2021**, *51*, 113–139. [[CrossRef](#)]
79. Yang, X.; Wan, Y.; Zheng, Y.; He, F.; Yu, Z.; Huang, J.; Gao, B. Surface functional groups of carbon-based adsorbents and their roles in the removal of heavy metals from aqueous solutions: A critical review. *Chem. Eng. J.* **2019**, *366*, 608–621. [[CrossRef](#)]
80. Tan, X.F.; Liu, Y.G.; Gu, Y.L.; Xu, Y.; Zeng, G.M.; Hu, X.J.; Li, J. Biochar-based nano-composites for the decontamination of wastewater: A review. *Bioresour. Technol.* **2016**, *212*, 318–333. [[CrossRef](#)]
81. Dai, L.; Lu, Q.; Zhou, H.; Shen, F.; Liu, Z.; Zhu, W.; Huang, H. Tuning oxygenated functional groups on biochar for water pollution control: A critical review. *J. Hazard. Mater.* **2021**, *420*, 126547. [[CrossRef](#)]
82. Yek, P.N.Y.; Peng, W.; Wong, C.C.; Liew, R.K.; Ho, Y.L.; Mahari, W.A.W.; Lam, S.S. Engineered biochar via microwave CO₂ and steam pyrolysis to treat carcinogenic Congo red dye. *J. Hazard. Mater.* **2020**, *395*, 122636. [[CrossRef](#)] [[PubMed](#)]
83. Park, J.H.; Wang, J.J.; Meng, Y.; Wei, Z.; DeLaune, R.D.; Seo, D.C. Adsorption/desorption behavior of cationic and anionic dyes by biochars prepared at normal and high pyrolysis temperatures. *Colloids Surf. A Physicochem. Eng. Asp.* **2019**, *572*, 274–282. [[CrossRef](#)]
84. Sterenzon, E.; Vadivel, V.K.; Gerchman, Y.; Luxbacher, T.; Narayanan, R.; Mamane, H. Effective Removal of Acid Dye in Synthetic and Silk Dyeing Effluent: Isotherm and Kinetic Studies. *ACS Omega* **2021**, *7*, 118–128. [[CrossRef](#)] [[PubMed](#)]
85. Chowdhury, M.F.; Khandaker, S.; Sarker, F.; Islam, A.; Rahman, M.T.; Awwal, M.R. Current treatment technologies and mechanisms for removal of indigo carmine dyes from wastewater: A review. *J. Mol. Liq.* **2020**, *318*, 114061. [[CrossRef](#)]
86. Eltaweil, A.S.; Mohamed, H.A.; Abd El-Monaem, E.M.; El-Subruti, G.M. Mesoporous magnetic biochar composite for enhanced adsorption of malachite green dye: Characterization, adsorption kinetics, thermodynamics and isotherms. *Adv. Powder Technol.* **2020**, *31*, 1253–1263. [[CrossRef](#)]
87. Yang, S.S.; Kang, J.H.; Xie, T.R.; He, L.; Xing, D.F.; Ren, N.Q.; Wu, W.M. Generation of high-efficient biochar for dye adsorption using frass of yellow mealworms (larvae of *Tenebrio molitor* Linnaeus) fed with wheat straw for insect biomass production. *J. Clean. Prod.* **2019**, *227*, 33–47. [[CrossRef](#)]
88. Yao, X.; Ji, L.; Guo, J.; Ge, S.; Lu, W.; Chen, Y.; Song, W. An abundant porous biochar material derived from wakame (*Undaria pinnatifida*) with high adsorption performance for three organic dyes. *Bioresour. Technol.* **2020**, *318*, 124082. [[CrossRef](#)]
89. Li, R.; Wang, J.J.; Gaston, L.A.; Zhou, B.; Li, M.; Xiao, R.; Zhang, X. An overview of carbothermal synthesis of metal–biochar composites for the removal of oxyanion contaminants from aqueous solution. *Carbon* **2018**, *129*, 674–687. [[CrossRef](#)]
90. Liu, P.; Liu, W.J.; Jiang, H.; Chen, J.J.; Li, W.W.; Yu, H.Q. Modification of bio-char derived from fast pyrolysis of biomass and its application in removal of tetracycline from aqueous solution. *Bioresour. Technol.* **2012**, *121*, 235–240. [[CrossRef](#)]
91. Shen, W.; Li, Z.; Liu, Y. Surface chemical functional groups modification of porous carbon. *Recent Pat. Chem. Eng.* **2008**, *1*, 27–40. [[CrossRef](#)]
92. Ahmaruzzaman, M. Biochar based nanocomposites for photocatalytic degradation of emerging organic pollutants from water and wastewater. *Mater. Res. Bull.* **2021**, *140*, 111262. [[CrossRef](#)]
93. Sun, J.; Lin, X.; Xie, J.; Zhang, Y.; Wang, Q.; Ying, Z. Facile synthesis of novel ternary g-C₃N₄/ferrite/biochar hybrid photocatalyst for efficient degradation of methylene blue under visible-light irradiation. *Colloids Surf. A Physicochem. Eng. Asp.* **2020**, *606*, 125556. [[CrossRef](#)]
94. Yu, F.; Tian, F.; Zou, H.; Ye, Z.; Peng, C.; Huang, J.; Gao, B. ZnO/biochar nanocomposites via solvent free ball milling for enhanced adsorption and photocatalytic degradation of methylene blue. *J. Hazard. Mater.* **2021**, *415*, 125511. [[CrossRef](#)] [[PubMed](#)]
95. Cheng, N.; Wang, B.; Wu, P.; Lee, X.; Xing, Y.; Chen, M.; Gao, B. Adsorption of emerging contaminants from water and wastewater by modified biochar: A review. *Environ. Pollut.* **2021**, *273*, 116448. [[CrossRef](#)]
96. Benis, K.Z.; Damuchali, A.M.; Soltan, J.; McPhedran, K.N. Treatment of aqueous arsenic—A review of biochar modification methods. *Sci. Total Environ.* **2020**, *739*, 139750. [[CrossRef](#)] [[PubMed](#)]
97. Barquilha, C.E.; Braga, M.C. Adsorption of organic and inorganic pollutants onto biochars: Challenges, operating conditions, and mechanisms. *Bioresour. Technol. Rep.* **2021**, *15*, 100728. [[CrossRef](#)]
98. Cho, H.H.; Wepasnick, K.; Smith, B.A.; Bangash, F.K.; Fairbrother, D.H.; Ball, W.P. Sorption of aqueous Zn [II] and Cd [II] by multiwall carbon nanotubes: The relative roles of oxygen-containing functional groups and graphenic carbon. *Langmuir* **2010**, *26*, 967–981. [[CrossRef](#)]

99. Wang, Y.; Zhong, B.; Shafi, M.; Ma, J.; Guo, J.; Wu, J.; Jin, H. Effects of biochar on growth, and heavy metals accumulation of moso bamboo (*Phyllostachy pubescens*), soil physical properties, and heavy metals solubility in soil. *Chemosphere* **2019**, *219*, 510–516. [[CrossRef](#)] [[PubMed](#)]
100. Li, Y.; Shao, J.; Wang, X.; Deng, Y.; Yang, H.; Chen, H. Characterization of modified biochars derived from bamboo pyrolysis and their utilization for target component (furfural) adsorption. *Energy Fuels* **2014**, *28*, 5119–5127. [[CrossRef](#)]
101. Peng, P.; Lang, Y.H.; Wang, X.M. Adsorption behavior and mechanism of pentachlorophenol on reed biochars: pH effect, pyrolysis temperature, hydrochloric acid treatment and isotherms. *Ecol. Eng.* **2016**, *90*, 225–233. [[CrossRef](#)]
102. Jin, Y.; Zhang, M.; Jin, Z.; Wang, G.; Li, R.; Zhang, X.; Wang, H. Characterization of biochars derived from various spent mushroom substrates and evaluation of their adsorption performance of Cu (II) ions from aqueous solution. *Environ. Res.* **2021**, *196*, 110323. [[CrossRef](#)] [[PubMed](#)]
103. Wei, D.; Li, B.; Huang, H.; Luo, L.; Zhang, J.; Yang, Y.; Zhou, Y. Biochar-based functional materials in the purification of agricultural wastewater: Fabrication, application and future research needs. *Chemosphere* **2018**, *197*, 165–180. [[CrossRef](#)]
104. Li, B.; Yang, L.; Wang, C.Q.; Zhang, Q.P.; Liu, Q.C.; Li, Y.D.; Xiao, R. Adsorption of Cd (II) from aqueous solutions by rape straw biochar derived from different modification processes. *Chemosphere* **2017**, *175*, 332–340. [[CrossRef](#)]
105. Sizmur, T.; Fresno, T.; Akgül, G.; Frost, H.; Moreno-Jiménez, E. Biochar modification to enhance sorption of inorganics from water. *Bioresour. Technol.* **2017**, *246*, 34–47. [[CrossRef](#)] [[PubMed](#)]
106. Cazetta, A.L.; Vargas, A.M.; Nogami, E.M.; Kunita, M.H.; Guilherme, M.R.; Martins, A.C.; Almeida, V.C. NaOH-activated carbon of high surface area produced from coconut shell: Kinetics and equilibrium studies from the methylene blue adsorption. *Chem. Eng. J.* **2011**, *174*, 117–125. [[CrossRef](#)]
107. Shen, Y.; Zhou, Y.; Fu, Y.; Zhang, N. Activated carbons synthesized from unaltered and pelletized biomass wastes for bio-tar adsorption in different phases. *Renew. Energy* **2020**, *146*, 1700–1709. [[CrossRef](#)]
108. Zheng, Y.; Wang, J.; Li, D.; Liu, C.; Lu, Y.; Lin, X.; Zheng, Z. Insight into the KOH/KMnO₄ activation mechanism of oxygen-enriched hierarchical porous biochar derived from biomass waste by in-situ pyrolysis for methylene blue enhanced adsorption. *J. Anal. Appl. Pyrolysis* **2021**, *158*, 105269. [[CrossRef](#)]
109. Dong, H.; Zhang, C.; Deng, J.; Jiang, Z.; Zhang, L.; Cheng, Y.; Zeng, G. Factors influencing degradation of trichloroethylene by sulfide-modified nanoscale zero-valent iron in aqueous solution. *Water Res.* **2018**, *135*, 1–10. [[CrossRef](#)] [[PubMed](#)]
110. Yang, X.; Xu, G.; Yu, H.; Zhang, Z. Preparation of ferric-activated sludge-based adsorbent from biological sludge for tetracycline removal. *Bioresour. Technol.* **2016**, *211*, 566–573. [[CrossRef](#)] [[PubMed](#)]
111. Navarathna, C.M.; Bombuwala Dewage, N.; Keeton, C.; Pennisson, J.; Henderson, R.; Lashley, B.; Mlsna, T. Biochar adsorbents with enhanced hydrophobicity for oil spill removal. *ACS Appl. Mater. Interfaces* **2020**, *12*, 9248–9260. [[CrossRef](#)] [[PubMed](#)]
112. Zulbadli, N.; Zaini, N.; Soon, L.Y.; Kang, T.Y.; Al-Harf, A.A.A.; Nasri, N.S.; Kamarudin, K.S.N. Acid-modified adsorbents from sustainable green-based materials for crude oil removal. *J. Adv. Res. Fluid Mech. Therm. Sci.* **2018**, *46*, 11–20.
113. Chen, L.; Jiang, X.; Xie, R.; Zhang, Y.; Jin, Y.; Jiang, W. A novel porous biochar-supported Fe-Mn composite as a persulfate activator for the removal of acid red 88. *Sep. Purif. Technol.* **2020**, *250*, 117232. [[CrossRef](#)]
114. Zhao, C.; Wang, B.; Theng, B.K.; Wu, P.; Liu, F.; Wang, S.; Zhang, X. Formation and mechanisms of nano-metal oxide-biochar composites for pollutants removal: A review. *Sci. Total Environ.* **2021**, *767*, 145305. [[CrossRef](#)]
115. Liu, J.; Huang, S.; Wang, T.; Mei, M.; Chen, S.; Li, J. Peroxydisulfate activation by digestate-derived biochar for azo dye degradation: Mechanism and performance. *Sep. Purif. Technol.* **2021**, *279*, 119687. [[CrossRef](#)]
116. Huang, Q.; Chen, C.; Zhao, X.; Bu, X.; Liao, X.; Fan, H.; Huang, Z. Malachite green degradation by persulfate activation with CuFe₂O₄@ biochar composite: Efficiency, stability and mechanism. *J. Environ. Chem. Eng.* **2021**, *9*, 105800. [[CrossRef](#)]
117. Liu, H.; Hu, M.; Zhang, H.; Wei, J. Biosynthesis of Stalk Biochar-nZVI and its Catalytic Reactivity in Degradation of Dyes by Persulfate. *Surf. Interfaces* **2022**, *31*, 102098. [[CrossRef](#)]
118. Zhao, Y.; Dai, H.; Ji, J.; Yuan, X.; Li, X.; Jiang, L.; Wang, H. Resource utilization of luffa sponge to produce biochar for effective degradation of organic contaminants through persulfate activation. *Sep. Purif. Technol.* **2022**, *288*, 120650. [[CrossRef](#)]
119. Gaspard, S.; Ncibi, M.C. (Eds.) *Activated Carbon from Biomass for Water Treatment. Biomass for Sustainable Applications: Pollution Remediation and Energy*; Royal Society of Chemistry: London, UK, 2013.
120. Kim, J.R.; Kan, E. Heterogeneous photocatalytic degradation of sulfamethoxazole in water using a biochar-supported TiO₂ photocatalyst. *J. Environ. Manag.* **2016**, *180*, 94–101. [[CrossRef](#)] [[PubMed](#)]
121. Ahmed, M.B.; Zhou, J.L.; Ngo, H.H.; Guo, W.; Chen, M. Progress in the preparation and application of modified biochar for improved contaminant removal from water and wastewater. *Bioresour. Technol.* **2016**, *214*, 836–851. [[CrossRef](#)] [[PubMed](#)]
122. Cha, J.S.; Park, S.H.; Jung, S.C.; Ryu, C.; Jeon, J.K.; Shin, M.C.; Park, Y.K. Production and utilization of biochar: A review. *J. Ind. Eng. Chem.* **2016**, *40*, 1–15. [[CrossRef](#)]
123. Panwar, N.L.; Pawar, A. Influence of activation conditions on the physicochemical properties of activated biochar: A review. *Biomass Convers. Biorefin.* **2020**, *12*, 925–947. [[CrossRef](#)]
124. Chia, C.H.; Downie, A.; Munroe, P. Characteristics of biochar: Physical and structural properties. In *Biochar for Environmental Management*; Routledge: London, UK, 2015; pp. 89–109.
125. Rajapaksha, A.U.; Vithanage, M.; Ahmad, M.; Seo, D.C.; Cho, J.S.; Lee, S.E.; Ok, Y.S. Enhanced sulfamethazine removal by steam-activated invasive plant-derived biochar. *J. Hazard. Mater.* **2015**, *290*, 43–50. [[CrossRef](#)] [[PubMed](#)]

126. Santos, R.M.; Santos, A.O.; Sussuchi, E.M.; Nascimento, J.S.; Lima, Á.S.; Freitas, L.S. Pyrolysis of mangaba seed: Production and characterization of bio-oil. *Bioresour. Technol.* **2015**, *196*, 43–48. [[CrossRef](#)] [[PubMed](#)]
127. Uchimiya, M.; Lima, I.M.; Klasson, K.T.; Wartelle, L.H. Contaminant immobilization and nutrient release by biochar soil amendment: Roles of natural organic matter. *Chemosphere* **2010**, *80*, 935–940. [[CrossRef](#)] [[PubMed](#)]
128. Hagemann, N.; Spokas, K.; Schmidt, H.P.; Kägi, R.; Böhrer, M.; Bucheli, T. Activated Carbon, Biochar and Charcoal: Linkages and Synergies across Pyrogenic Carbon's ABCs. *Water* **2018**, *10*, 182. [[CrossRef](#)]
129. Jellali, S.; Khiari, B.; Usman, M.; Hamdi, H.; Charabi, Y.; Jeguirim, M. Sludge-derived biochars: A review on the influence of synthesis conditions on pollutants removal efficiency from wastewaters. *Renew. Sustain. Energy Rev.* **2021**, *144*, 111068. [[CrossRef](#)]
130. Méndez, A.; Gascó, G.; Freitas, M.M.A.; Siebielec, G.; Stuczynski, T.; Figueiredo, J.L. Preparation of carbon-based adsorbents from pyrolysis and air activation of sewage sludges. *Chem. Eng. J.* **2005**, *108*, 169–177. [[CrossRef](#)]
131. Sewu, D.D.; Jung, H.; Kim, S.S.; Lee, D.S.; Woo, S.H. Decolorization of cationic and anionic dye-laden wastewater by steam-activated biochar produced at an industrial-scale from spent mushroom substrate. *Bioresour. Technol.* **2019**, *277*, 77–86. [[CrossRef](#)]
132. Jin, H.; Capareda, S.; Chang, Z.; Gao, J.; Xu, Y.; Zhang, J. Biochar pyrolytically produced from municipal solid wastes for aqueous As (V) removal: Adsorption property and its improvement with KOH activation. *Bioresour. Technol.* **2014**, *169*, 622–629. [[CrossRef](#)] [[PubMed](#)]
133. Zhang, Q.; Wang, J.; Lyu, H.; Zhao, Q.; Jiang, L.; Liu, L. Ball-milled biochar for galaxolide removal: Sorption performance and governing mechanisms. *Sci. Total Environ.* **2019**, *659*, 1537–1545. [[CrossRef](#)] [[PubMed](#)]
134. Arif, M.; Liu, G.; Yousaf, B.; Ahmed, R.; Irshad, S.; Ashraf, A.; Rashid, M.S. Synthesis, characteristics and mechanistic insight into the clays and clay minerals-biochar surface interactions for contaminants removal—A review. *J. Clean. Prod.* **2021**, *310*, 127548. [[CrossRef](#)]
135. Zhao, Y.; Yuan, X.; Li, X.; Jiang, L.; Wang, H. Burgeoning prospects of biochar and its composite in persulfate-advanced oxidation process. *J. Hazard. Mater.* **2021**, *409*, 124893. [[CrossRef](#)] [[PubMed](#)]
136. Peterson, S.C.; Jackson, M.A.; Kim, S.; Palmquist, D.E. Increasing biochar surface area: Optimization of ball milling parameters. *Powder Technol.* **2012**, *228*, 115–120. [[CrossRef](#)]
137. Lyu, H.; Gao, B.; He, F.; Zimmerman, A.R.; Ding, C.; Huang, H.; Tang, J. Effects of ball milling on the physicochemical and sorptive properties of biochar: Experimental observations and governing mechanisms. *Environ. Pollut.* **2018**, *233*, 54–63. [[CrossRef](#)]
138. Zheng, Y.; Wan, Y.; Chen, J.; Chen, H.; Gao, B. MgO modified biochar produced through ball milling: A dual-functional adsorbent for removal of different contaminants. *Chemosphere* **2020**, *243*, 125344. [[CrossRef](#)]
139. Sewu, D.D.; Tran, H.N.; Ohemeng-Boahen, G.; Woo, S.H. Facile magnetic biochar production route with new goethite nanoparticle precursor. *Sci. Total Environ.* **2020**, *717*, 137091. [[CrossRef](#)]
140. Qiu, Y.; Zhang, Q.; Wang, Z.; Gao, B.; Fan, Z.; Li, M.; Zhong, M. Degradation of anthraquinone dye reactive blue 19 using persulfate activated with Fe/Mn modified biochar: Radical/non-radical mechanisms and fixed-bed reactor study. *Sci. Total Environ.* **2021**, *758*, 143584. [[CrossRef](#)]
141. Zhao, F.; Shan, R.; Li, W.; Zhang, Y.; Yuan, H.; Chen, Y. Synthesis, characterization, and dye removal of ZnCl₂-modified biochar derived from pulp and paper sludge. *ACS Omega* **2021**, *6*, 34712–34723. [[CrossRef](#)]
142. Feng, Z.; Yuan, R.; Wang, F.; Chen, Z.; Zhou, B.; Chen, H. Preparation of magnetic biochar and its application in catalytic degradation of organic pollutants: A review. *Sci. Total Environ.* **2021**, *765*, 142673. [[CrossRef](#)]
143. Reddy, D.H.K.; Lee, S.M. Magnetic biochar composite: Facile synthesis, characterization, and application for heavy metal removal. *Colloids Surf. A Physicochem. Eng. Asp.* **2014**, *454*, 96–103. [[CrossRef](#)]
144. Qu, S.; Huang, F.; Yu, S.; Chen, G.; Kong, J. Magnetic removal of dyes from aqueous solution using multi-walled carbon nanotubes filled with Fe₂O₃ particles. *J. Hazard. Mater.* **2008**, *160*, 643–647. [[CrossRef](#)]
145. Thines, K.R.; Abdullah, E.C.; Mubarak, N.M.; Ruthiraan, M. Synthesis of magnetic biochar from agricultural waste biomass to enhancing route for waste water and polymer application: A review. *Renew. Sustain. Energy Rev.* **2017**, *67*, 257–276. [[CrossRef](#)]
146. Theydan, S.K.; Ahmed, M.J. Adsorption of methylene blue onto biomass-based activated carbon by FeCl₃ activation: Equilibrium, kinetics, and thermodynamic studies. *J. Anal. Appl. Pyrolysis* **2012**, *97*, 116–122. [[CrossRef](#)]
147. Wang, S.; Gao, B.; Zimmerman, A.R.; Li, Y.; Ma, L.; Harris, W.G.; Migliaccio, K.W. Removal of arsenic by magnetic biochar prepared from pinewood and natural hematite. *Bioresour. Technol.* **2015**, *175*, 391–395. [[CrossRef](#)]
148. Baig, S.A.; Zhu, J.; Muhammad, N.; Sheng, T.; Xu, X. Effect of synthesis methods on magnetic Kans grass biochar for enhanced As (III, V) adsorption from aqueous solutions. *Biomass Bioenergy* **2014**, *71*, 299–310. [[CrossRef](#)]
149. Han, Y.; Cao, X.; Ouyang, X.; Sohi, S.P.; Chen, J. Adsorption kinetics of magnetic biochar derived from peanut hull on removal of Cr (VI) from aqueous solution: Effects of production conditions and particle size. *Chemosphere* **2016**, *145*, 336–341. [[CrossRef](#)] [[PubMed](#)]
150. Guo, L.; Zhao, L.; Tang, Y.; Zhou, J.; Shi, B. An iron-based biochar for persulfate activation with highly efficient and durable removal of refractory dyes. *J. Environ. Chem. Eng.* **2022**, *10*, 106979. [[CrossRef](#)]
151. Abodif, A.M.; Meng, L.; Ma, S.; Ahmed, A.S.; Belvett, N.; Wei, Z.Z.; Ning, D. Mechanisms and models of adsorption: TiO₂-supported biochar for removal of 3,4-dimethylaniline. *ACS Omega* **2020**, *5*, 13630–13640. [[CrossRef](#)]
152. Deng, H.; Li, A.; Ye, C.; Sheng, L.; Li, Z.; Jiang, Y. Green Removal of Various Pollutants by Microsphere Adsorption: Material Characterization and Adsorption Behavior. *Energy Fuels* **2020**, *34*, 16330–16340. [[CrossRef](#)]

153. Liu, S.; Shen, C.; Wang, Y.; Huang, Y.; Hu, X.; Li, B.; Zhang, H. Development of CO₂/H₂O activated biochar derived from pine pyrolysis: Application in methylene blue adsorption. *J. Chem. Technol. Biotechnol.* **2022**, *97*, 885–893. [[CrossRef](#)]
154. Liu, S.; Li, J.; Xu, S.; Wang, M.; Zhang, Y.; Xue, X. A modified method for enhancing adsorption capability of banana pseudostem biochar towards methylene blue at low temperature. *Bioresour. Technol.* **2019**, *282*, 48–55. [[CrossRef](#)]
155. Hoslett, J.; Ghazal, H.; Mohamad, N.; Jouhara, H. Removal of methylene blue from aqueous solutions by biochar prepared from the pyrolysis of mixed municipal discarded material. *Sci. Total Environ.* **2020**, *714*, 136832. [[CrossRef](#)]
156. Sahu, S.; Pahi, S.; Tripathy, S.; Singh, S.K.; Behera, A.; Sahu, U.K.; Patel, R.K. Adsorption of methylene blue on chemically modified lychee seed biochar: Dynamic, equilibrium, and thermodynamic study. *J. Mol. Liq.* **2020**, *315*, 113743. [[CrossRef](#)]
157. Chen, X.L.; Li, F.; Chen, H.; Wang, H.; Li, G. Fe₂O₃/TiO₂ functionalized biochar as a heterogeneous catalyst for dyes degradation in water under Fenton processes. *J. Environ. Chem. Eng.* **2020**, *8*, 103905. [[CrossRef](#)]
158. Liu, X.J.; Li, M.F.; Singh, S.K. Manganese-modified lignin biochar as adsorbent for removal of methylene blue. *J. Mater. Res. Technol.* **2021**, *12*, 1434–1445. [[CrossRef](#)]
159. Bal, D.; Özer, Ç.; İmamoğlu, M. Green and ecofriendly biochar preparation from pumpkin peel and its usage as an adsorbent for methylene blue removal from aqueous solutions. *Water Air Soil Pollut.* **2021**, *232*, 457. [[CrossRef](#)]
160. Pandey, D.; Daverey, A.; Dutta, K.; Yata, V.K.; Arunachalam, K. Valorization of waste pine needle biomass into biosorbents for the removal of methylene blue dye from water: Kinetics, equilibrium and thermodynamics study. *Environ. Technol. Innov.* **2022**, *25*, 102200. [[CrossRef](#)]
161. Pandey, D.; Daverey, A.; Dutta, K.; Arunachalam, K. Bioremoval of toxic malachite green from water through simultaneous decolorization and degradation using laccase immobilized biochar. *Chemosphere* **2022**, *297*, 134126. [[CrossRef](#)]
162. Eldeeb, T.M.; Aigbe, U.O.; Ukhurebor, K.E.; Onyancha, R.B.; El-Nemr, M.A.; Hassaan, M.A.; El Nemr, A. Adsorption of methylene blue (MB) dye on ozone, purified and sonicated sawdust biochars. *Biomass Convers. Biorefin.* **2022**, 1–23. [[CrossRef](#)]
163. Zhao, Z.; Zhou, W. Insight into interaction between biochar and soil minerals in changing biochar properties and adsorption capacities for sulfamethoxazole. *Environ. Pollut.* **2019**, *245*, 208–217. [[CrossRef](#)] [[PubMed](#)]
164. Lu, J.; Yang, Y.; Liu, P.; Li, Y.; Huang, F.; Zeng, L.; Hou, B. Iron-montmorillonite treated corn straw biochar: Interfacial chemical behavior and stability. *Sci. Total Environ.* **2020**, *708*, 134773. [[CrossRef](#)]
165. Han, H.; Rafiq, M.K.; Zhou, T.; Xu, R.; Mašek, O.; Li, X. A critical review of clay-based composites with enhanced adsorption performance for metal and organic pollutants. *J. Hazard. Mater.* **2019**, *369*, 780–796. [[CrossRef](#)]
166. Khandelwal, N.; Tiwari, E.; Singh, N.; Darbha, G.K. Heterogeneously Porous Multiadsorbent Clay–Biochar Surface to Support Redox-Sensitive Nanoparticles: Applications of Novel Clay–Biochar–Nanoscale Zerovalent Iron Nanotrident (C-BC-nZVI) in Continuous Water Filtration. *ACS EST Water* **2021**, *1*, 641–652. [[CrossRef](#)]
167. Lakshmi, D.; Akhil, D.; Kartik, A.; Gopinath, K.P.; Arun, J.; Bhatnagar, A.; Muthusamy, G. Artificial intelligence (AI) applications in adsorption of heavy metals using modified biochar. *Sci. Total Environ.* **2021**, *801*, 149623. [[CrossRef](#)]
168. Mishra, P.; Gupta, C. Cookies in a Cross-site scripting: Type, Utilization, Detection, Protection and Remediation. In Proceedings of the 2020 8th International Conference on Reliability, Infocom Technologies and Optimization (Trends and Future Directions) (ICRITO), Noida, India, 4–5 June 2020; pp. 1056–1059. [[CrossRef](#)]
169. Babaei, A.A.; Khataee, A.; Ahmadpour, E.; Sheydaei, M.; Kakavandi, B.; Alaei, Z. Optimization of cationic dye adsorption on activated spent tea: Equilibrium, kinetics, thermodynamic and artificial neural network modeling. *Korean J. Chem. Eng.* **2016**, *33*, 1352–1361. [[CrossRef](#)]
170. Moosavi, S.; Manta, O.; El-Badry, Y.A.; Hussein, E.E.; El-Bahy, Z.M.; Mohd Fawzi, N.F.B.; Moosavi, S.M.H. A study on machine learning methods' application for dye adsorption prediction onto agricultural waste activated carbon. *Nanomaterials* **2021**, *11*, 2734. [[CrossRef](#)]
171. Alam, G.; Ihsanullah, I.; Naushad, M.; Sillanpää, M. Applications of artificial intelligence in water treatment for optimization and automation of adsorption processes: Recent advances and prospects. *Chem. Eng. J.* **2022**, *427*, 130011. [[CrossRef](#)]
172. Taoufik, N.; Boumya, W.; Achak, M.; Chennouk, H.; Dewil, R.; Barka, N. The state of art on the prediction of efficiency and modeling of the processes of pollutants removal based on machine learning. *Sci. Total Environ.* **2022**, *807*, 150554. [[CrossRef](#)]
173. Beck, D.A.; Carothers, J.M.; Subramanian, V.R.; Pfaendtner, J. Data science: Accelerating innovation and discovery in chemical engineering. *AIChE J.* **2016**, *62*, 1402–1416. [[CrossRef](#)]
174. Ghaedi, A.M.; Vafaei, A. Applications of artificial neural networks for adsorption removal of dyes from aqueous solution: A review. *Adv. Colloid Interface Sci.* **2017**, *245*, 20–39. [[CrossRef](#)]
175. Aber, S.; Daneshvar, N.; Soroureddin, S.M.; Chabok, A.; Asadpour-Zeynali, K. Study of acid orange 7 removal from aqueous solutions by powdered activated carbon and modeling of experimental results by artificial neural network. *Desalination* **2007**, *211*, 87–95. [[CrossRef](#)]